

Targeted therapy in patients with PIK3CA-related overgrowth syndrome

Quitterie Venot¹, Thomas Blanc^{1,2,3,21}, Smail Hadj Rabia^{2,4,5,21}, Laureline Berteloot^{5,6}, Sophia Ladraa¹, Jean-Paul Duong^{2,7}, Estelle Blanc⁸, Simon C. Johnson⁹, Clément Huguin¹, Olivia Boccarà⁴, Sabine Sarnacki^{2,3}, Nathalie Boddaert^{2,5,6}, Stephanie Pannier^{2,10}, Frank Martinez¹¹, Sato Magassa¹, Junna Yamaguchi¹, Bertrand Knebelmann^{1,2,11}, Pierre Merville^{12,13}, Nicolas Grenier¹⁴, Dominique Joly^{1,2,11}, Valérie Cormier-Daire^{2,5,15}, Caroline Michot^{2,5,15}, Christine Bole-Feysot⁵, Arnaud Picard^{2,16}, Véronique Soupre¹⁶, Stanislas Lyonnet^{2,5,15}, Jeremy Sadoine¹⁷, Lotfi Slimani¹⁷, Catherine Chaussain^{2,17}, Cécile Laroche-Raynaud¹⁸, Laurent Guibaud¹⁹, Christine Broissand²⁰, Jeanne Amiel^{2,5,15}, Christophe Legendre^{1,2,11}, Fabiola Terzi^{1,2} & Guillaume Canaud^{1,2,11*}

CLOVES syndrome (congenital lipomatous overgrowth, vascular malformations, epidermal naevi, scoliosis/skeletal and spinal syndrome) is a genetic disorder that results from somatic, mosaic gain-of-function mutations of the *PIK3CA* gene, and belongs to the spectrum of *PIK3CA*-related overgrowth syndromes (PROS). This rare condition has no specific treatment and a poor survival rate. Here, we describe a postnatal mouse model of PROS/CLOVES that partially recapitulates the human disease, and demonstrate the efficacy of BYL719, an inhibitor of *PIK3CA*, in preventing and improving organ dysfunction. On the basis of these results, we used BYL719 to treat nineteen patients with PROS. The drug improved the disease symptoms in all patients. Previously intractable vascular tumours became smaller, congestive heart failure was improved, hemihypertrophy was reduced, and scoliosis was attenuated. The treatment was not associated with any substantial side effects. In conclusion, this study provides the first direct evidence supporting *PIK3CA* inhibition as a promising therapeutic strategy in patients with PROS.

The phosphoinositide-3 kinases (PI(3)Ks) are key lipid kinases that control signalling pathways involved in cell proliferation, motility, survival and metabolism¹. Class I PI(3)K contains four catalytic isoforms (p110 α , p110 β , p110 δ and p110 γ), which carry out non-redundant signalling functions¹. *PIK3CA* encodes the 110-kD catalytic α -subunit of PI(3)K (p110 α), which converts phosphatidylinositol (3,4)-bisphosphate (PtdIns(3,4)P₂) to phosphatidylinositol (3,4,5)-triphosphate (PtdIns(3,4,5)P₃). This leads to the activation of PDK1, which phosphorylates AKT on Thr308^{2,3}. AKT, through the phosphorylation and inhibition of tuberous sclerosis complex 2 (TSC2), activates the kinase mechanistic target of rapamycin complex 1 (mTORC1)⁴. *PIK3CA* is a master regulator of cell growth and other pathways, including the Rho/Rac1 signalling cascade. PROS are caused by post-zygotic mosaic gain-of-function mutations in the *PIK3CA* gene⁵, resulting in mosaic *PIK3CA* activation, which drives various patient phenotypes, ranging from isolated macrodactyly to CLOVES syndrome⁶. Notably, an increasing number of phenotypes has been included in PROS as a result of the identification of *PIK3CA* mutations in previously uncharacterized overgrowth syndromes. Thus, the prevalence of PROS is difficult to estimate owing to the variability of correct clinical diagnoses and the broad phenotypic spectrum of the disorders⁶.

There are no animal models of PROS that can be used to understand its pathophysiology, and no specific treatments for patients^{6,7}. Patients with PROS mainly receive supportive care based on debulking and

mutating surgery, sclerotherapy, and psychological and nutritional support. Inhibition of mTORC seems to improve lymphatic malformations in some patients but is associated with many side effects^{5,8}.

Several *PIK3CA* inhibitors are under development as treatments for oncological conditions, where gain-of-function mutations in *PIK3CA* are observed⁹. Among them, BYL719 shows dose- and time-dependent inhibition of the PI3K/AKT pathway in *PIK3CA*-dependent xenograft tumour models^{10,11}. As BYL719 is currently under investigation in clinical trials in patients with *PIK3CA*-dependent tumours and has good tolerability¹², we decided to explore its therapeutic potential in PROS.

A mouse model of PROS/CLOVES

We started by developing a mouse model of PROS/CLOVES. To this end, we took advantage of the transgenic mouse strain, *R26StopFLP110*^{*13,14}, which, after breeding with Cre recombinase mice, express a dominant active *PI3KCA* transgene (Extended Data Fig. 1a, b). *R26StopFLP110*^{*} mice were crossed with *CAGG-CreER* mice¹⁵ to generate *PIK3CA*^{CAGG-CreER} animals that ubiquitously express *PIK3CA* upon tamoxifen administration, and EGFP to monitor Cre recombination. Three-week-old mice were treated with a single dose of 40 mg kg⁻¹ tamoxifen to induce Cre recombination¹⁵. EGFP staining revealed that Cre recombination occurred in 25.5 \pm 8.3% of splenocytes (Extended Data Fig. 1c). After tamoxifen administration, we observed that the *PIK3CA*^{CAGG-CreER} mice started to rapidly die with 50% of mortality at

¹INSERM U1151, Institut Necker Enfants Malades, Paris, France. ²Université Paris Descartes, Sorbonne Paris Cité, Paris, France. ³Service de Chirurgie Viscérale Pédiatrique, Hôpital Necker-Enfants Malades, AP-HP, Paris, France. ⁴Service de Dermatologie Pédiatrique, Hôpital Necker-Enfants Malades, AP-HP, Paris, France. ⁵UMR-1163 Institut Imagine, Hôpital Necker-Enfants Malades, AP-HP, Paris, France. ⁶Département de Radiologie Pédiatrique, Hôpital Necker-Enfants Malades, AP-HP, Paris, France. ⁷Département d'Anatomopathologie, Hôpital Necker-Enfants Malades, AP-HP, Paris, France. ⁸Département de Médecine Nucléaire, Hôpital Marie Lannelongue, Le Plessis Robinson, France. ⁹Department of Integrative Brain Research, Seattle Children's Research Institute, Seattle, WA, USA. ¹⁰Service d'Orthopédie Pédiatrique, Hôpital Necker-Enfants Malades, AP-HP, Paris, France. ¹¹Service de Néphrologie Transplantation Adultes, Hôpital Necker-Enfants Malades, AP-HP, Paris, France. ¹²Service de Néphrologie, Transplantation, Dialyse, Aphèreses, Centre Hospitalier Universitaire Pellegrin, Bordeaux, France. ¹³UMR CNRS 5164, Immuno ConcEpT, CNRS, Bordeaux, France. ¹⁴Service d'Imagerie Diagnostique et Interventionnelle de l'Adulte, Centre Hospitalier Universitaire Pellegrin, Bordeaux, France. ¹⁵Service de Génétique Médicale, Hôpital Necker-Enfants Malades, AP-HP, Paris, France. ¹⁶Service de Chirurgie Maxillo-faciale et Chirurgie Plastique, Hôpital Necker-Enfants Malades, AP-HP, Paris, France. ¹⁷Laboratory EA 2496 Orofacial Pathologies, Imaging and Biotherapies, Montrouge, France. ¹⁸Service de Neuropédiatrie, Hôpital de la Mère et de l'Enfant, Limoges, France. ¹⁹Service d'Imagerie Pédiatrique, Hôpital Femme-Mère-Enfant, Bron, France. ²⁰Pharmacie, Hôpital Necker-Enfants Malades, AP-HP, Paris, France. ²¹These authors contributed equally: Thomas Blanc, Smail Hadj Rabia. *e-mail: guillaume.canaud@inserm.fr

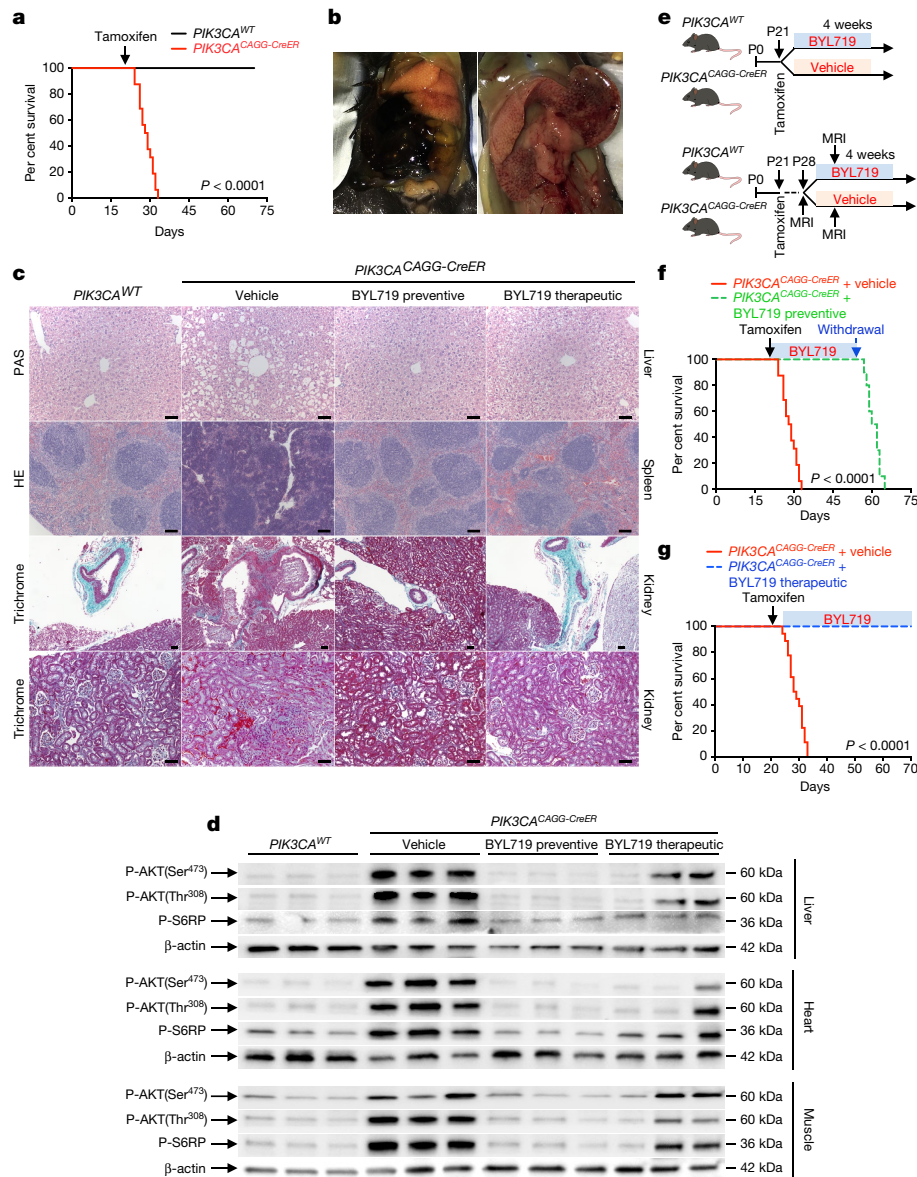


Fig. 1 | Characterization of the PROS mouse model and efficacy of BYL719. **a**, Kaplan–Meier survival curves of *PIK3CA*^{WT} and *PIK3CA*^{CAGG-CreER} mice ($n = 16$ mice per group) after tamoxifen administration (log-rank test, $P < 0.0001$). **b**, Representative necropsy examination pictures of *PIK3CA*^{CAGG-CreER} mice. The mice displayed sudden intra-abdominal and spontaneous hepatic haemorrhage ($n = 16$ mice). **c**, Morphology of livers (top), spleens (middle) and kidneys (bottom two rows) from *PIK3CA*^{WT} and *PIK3CA*^{CAGG-CreER} mice that were treated with or without BYL719 directly after *Cre* induction (preventive) or seven days later (therapeutic) ($n = 8$ mice per group). **d**, Western blot

of P-AKT (Ser⁴⁷³), P-AKT (Thr³⁰⁸) and P-S6RP in liver, heart and muscles, respectively, from *PIK3CA*^{WT} and *PIK3CA*^{CAGG-CreER} mice treated with or without BYL719 directly after *Cre* induction (preventive) or seven days later (therapeutic) ($n = 8$ mice per group). **e**, Experimental design. **f**, Kaplan–Meier survival curves of *PIK3CA*^{CAGG-CreER} mice treated with or without BYL719 after tamoxifen administration ($n = 16$ mice per group). After 40 days, BYL719 treatment was withdrawn (log-rank test, $P < 0.0001$). **g**, Kaplan–Meier survival curves of *PIK3CA*^{CAGG-CreER} mice treated with or without BYL719 ($n = 12$ mice per group) seven days after tamoxifen administration (log-rank test, $P < 0.0001$). Scale bars, 20 μm .

day 9 (Fig. 1a). Death occurred suddenly in most cases, with necropsy revealing intra-abdominal and hepatic haemorrhages (Fig. 1b). Whole body magnetic resonance imaging (MRI) showed scoliosis, vessel abnormalities, kidney cysts, and muscle hypertrophy (Extended Data Fig. 1e, left and middle columns). Histological examination revealed multiple organ abnormalities, including severe liver steatosis with vessel disorganization, loss of spleen microarchitecture integrity, spontaneous haemorrhages and fibrosis of the kidney with aberrant vessels (Fig. 1c, Extended Data Fig. 2a, b). We observed a high number of proliferating cells in all the affected organs of the *PIK3CA*^{CAGG-CreER} mice, as assessed by Ki67 immunostaining (Extended Data Fig. 3a). By contrast, we failed to detect any change in apoptosis (Extended Data Fig. 3b) or senescence (Extended Data Fig. 4a, b). To further characterize the previously reported vessel malformations, we performed CD34 and

CD31 immunostaining, which confirmed the presence of severe vessel dilation (Extended Data Fig. 2c). Similarly, podoplanin and LYVE-1 confirmed expansion of lymphatic vessels (Extended Data Fig. 2d, e). We confirmed that mutant p110 α (p110*) was expressed in all affected organs (Extended Data Fig. 5a). Notably, we did not detect expression in the brain or lungs (Extended Data Fig. 5b), consistent with the normal histology of these organs (data not shown). Western blot and immunofluorescence studies showed AKT/mTORC pathway activation in all the examined organs (Fig. 1d and Extended Data Figs. 5c–e, 6). In transfected HeLa cells, the p110* mutant had a stronger effect on AKT/mTORC pathway activation than did the *c.3140A>G* (H1047R) and *c.1633G>A* (E545K) mutations from patients used in previously reported models^{16,17} (Extended Data Fig. 7), which may explain the increased phenotypical severity observed in our model.

BYL719 prevents the PROS/CLOVES phenotype

We next studied the effect of BYL719 on *PIK3CA*^{CAGG-CreER} mice. Initially, BYL719 was administered orally each day starting on the day of *Cre* induction (Fig. 1e). Whereas all placebo-treated *PIK3CA*^{CAGG-CreER} mice died within 15 days, all BYL719-treated *PIK3CA*^{CAGG-CreER} mice were alive after 40 days and had an overtly normal appearance (Fig. 1f). Histological examination at 40 days showed that the BYL719 treated mice had preserved tissues (Fig. 1c and Extended Data Fig. 2a) and normal vessels (Extended Data Fig. 2c). Mechanistically, we observed a strong reduction of proliferation in *PIK3CA*^{CAGG-CreER} mice treated with BYL719 (Extended Data Fig. 3a), whereas senescence and apoptosis did not change (Extended Data Figs. 3b, 4a, b). Western blot and immunofluorescence analyses confirmed that PI3KCA pathway activation was effectively inhibited (Fig. 1d and Extended Data Fig. 5c–e, 6). However, interruption of treatment 40 days after *Cre* recombination led to the rapid death of all *PIK3CA*^{CAGG-CreER} mice (median survival 9.8 days after withdrawal of the drug; Fig. 1f).

Next, we administered either placebo or BYL719 to *PIK3CA*^{CAGG-CreER} mice seven days after *Cre* induction (Fig. 1e), when tissue abnormalities were already detected by MRI (Extended Data Fig. 1e). BYL719 treatment improved the survival of the *PIK3CA*^{CAGG-CreER} mice (Fig. 1g). MRI performed 12 days after the start of treatment (19 days after *Cre* induction) showed improvements in scoliosis, muscle hypertrophy, and vessel malformations (Extended Data Fig. 1e). Histological analysis of BYL719-treated mice revealed only minor tissue changes compared to wild-type mice (Fig. 1c, Extended Data Fig. 2a). BYL719 administration strongly reduced cell proliferation in all affected organs (Extended Data Fig. 3a), and western blot and immunofluorescence analyses confirmed PI3KCA pathway inhibition (Fig. 1d, Extended Data Figs. 5c–e, 6).

To try to reproduce more faithfully the lower mosaicism observed in patients¹⁸, we used a single dose of 4 mg kg⁻¹ tamoxifen to induce *Cre* recombination. We confirmed that a lower dose of tamoxifen induced a lower rate of mosaicism by fluorescence-activated cell sorting (FACS; 4.1 ± 1.3%, Extended Data Fig. 1d). The mice survived for two months and then died with multiple phenotypic abnormalities. In addition to organomegaly¹⁹, these mice progressively developed asymmetrical overgrowth of extremities, disseminated voluminous tumours and visible subcutaneous vascular abnormalities (Fig. 2a). Histological examination of the tumours revealed the same lesions observed in patients with PROS (lipomatous tumours (Fig. 2b) and severe vascular lesions mixing venous and arterial vessels (Fig. 2c–e). More precisely, we observed ecstatic venous channels with a thin endothelial cell lining, surrounded by sparse, erratically distributed vascular smooth muscle cells and a disorganized extracellular matrix, as is seen in PROS/CLOVES (Fig. 2e). Immunofluorescence and immunohistochemistry studies confirmed the increase in cell proliferation and activation of the AKT/mTORC pathway (Fig. 2f, Extended Data Fig. 7b).

Once the lesions were clinically visible, we treated the low-dose *PIK3CA*^{CAGG-CreER} mice with BYL719. Remarkably, the treatment led to the reduction and disappearance of all visible tumours within two weeks, with body weight loss (Fig. 2g, Extended Data Fig. 8a). Computerized tomography (CT) scanning showed a marked and rapid reduction in tumour volume (−83.96 ± 2.81%), with no change in fat content (Extended Data Fig. 8b).

Notably, withdrawal of BYL719 led to the recurrence of tumours and the development of asymmetric extremity hypertrophy within four weeks (Fig. 2h, Extended Data Fig. 7c). These data suggest that continuous administration of BYL719 can relieve PROS symptoms at different stages by inhibiting hyperactive PI3KCA signalling.

BYL719 is more effective than rapamycin

As the mTOR inhibitor rapamycin has shown some efficacy in treating vascular malformation²⁰, we tested its efficacy in our mouse models. In the first *PIK3CA*^{CAGG-CreER} mouse model, which received 40 mg kg⁻¹ tamoxifen, rapamycin improved survival (Extended Data Fig. 9a). However, it did not improve organ abnormalities such as liver

and spleen disorganization with aberrant vascularization (Extended Data Fig. 9b, c). Western blot analysis revealed that rapamycin blocked mTORC1 activity but, as previously reported²¹, did not inhibit mTORC2 as assessed by the persistent phosphorylation of AKT on Ser473 in all the examined organs (Extended Data Fig. 9d). Similarly, in the *PIK3CA*^{CAGG-CreER} mouse model that received 4 mg kg⁻¹ tamoxifen, rapamycin treatment did not reduce tumour growth significantly (Extended Data Fig. 9e). In parallel to these studies, we exposed primary mouse fibroblasts from PROS mice to either rapamycin or BYL719. Mutant p110* overexpression led to the phosphorylation of AKT on both Ser473 and Thr308 as well as the phosphorylation of S6RP (Extended Data Fig. 10a, b). By contrast, we could not detect any activation of the p38 and p44/42 MAP kinase pathway. Notably, unlike rapamycin, BYL719 blocked AKT phosphorylation on both Thr308 and Ser473, suggesting that the beneficial effect of BYL719 could be driven by more complete blockage of AKT (Extended Data Fig. 10a, b). These results confirmed that BYL719 could be a good therapeutic option even for patients for whom rapamycin is not an effective option.

BYL719 in two patients with CLOVES syndrome

We administered BYL719 under compassionate care protocols to two patients, one adult and one child, who were suffering from extremely severe clinical manifestations of PROS/CLOVES syndrome with therapeutic failure and life-threatening complications. Patient 1 was a 29-year-old man with *PIK3CA* c.3140A>G (H1047R) mutation (11% mosaicism). He presented left leg hypertrophy, scoliosis, multiple naevi, and extremely severe vascular malformations (Fig. 3a–c). He had previously undergone multiple tumour debulking surgeries and angiographies. He became paraplegic at the age of 20 owing to spinal cord compression and required bladder stenting. He developed progressively worsening, drug-resistant, severe systolic heart failure with a measured cardiac output of 181 min⁻¹ m⁻² (normal < 3.51 min⁻¹ m⁻²). Consistently, the brain natriuretic peptide (BNP) level was over 2,500 pg ml⁻¹ (normal < 100 pg ml⁻¹) (Fig. 3d). Over five years, the patient received different doses of rapamycin²² to limit vascular tumour growth progression, but this had no overt effects on his abdominal and dorsal vascular tumours. Finally, the patient developed kidney dysfunction with severe proteinuria. A kidney biopsy revealed glomerular lesions with extensive fibrosis. Such lesions may be the result of heart dysfunction, the administration of rapamycin^{5,8}, and/or *PIK3CA* mutations in the kidney epithelial cells. CT scan (Fig. 3b) and MRI (Fig. 3e) analyses showed severe vascular malformations, while positron emission tomography (PET) scan analysis was negative. Karnofsky and Eastern cooperative oncology group (ECOG) scores, which indicate general health status^{23,24}, were 20% and 4, respectively. Owing to the severity of the case and poor prognosis, the physicians, surgeons, and radiologists decided to stop any interventional treatment and to provide the patient with only supportive and palliative care. His estimated life expectancy was less than a few months. One month after rapamycin washout, daily oral BYL719 was started at 250 mg per day, the lowest dose used in clinical trials. We observed a rapid improvement in the general status of the patient, as well as a progressive reduction in tumour size, venous dilations and skin lesions (Fig. 3a). He lost 25 kg in 18 months due to oedema clearance but also to a major reduction in vascular tumour abnormalities (Fig. 3c). His thorax and abdomen circumferences were reduced by 25% and 39%, respectively, over 18 months (Fig. 3c). CT scan and MRI analyses confirmed global vascular tumour shrinkage (72% volume decrease at 18 months), as well as disappearance of subcutaneous infiltration (Fig. 3b, e). The effect of the drug on heart function was remarkable, with complete correction of BNP levels within 4 weeks (Fig. 3d). Cardiac output decreased to 31 min⁻¹ m⁻², and his heart size reduced by 25% (Fig. 3b). The left ventricular mass index to body surface area decreased from 250 g m⁻² to 148 g m⁻². Renal function also improved rapidly, with estimated glomerular filtration rate increasing from 33 to 52 ml min⁻¹ per 1.73 m² (Fig. 3d). The hypertrophy of the left leg was also reduced (Fig. 3a). We

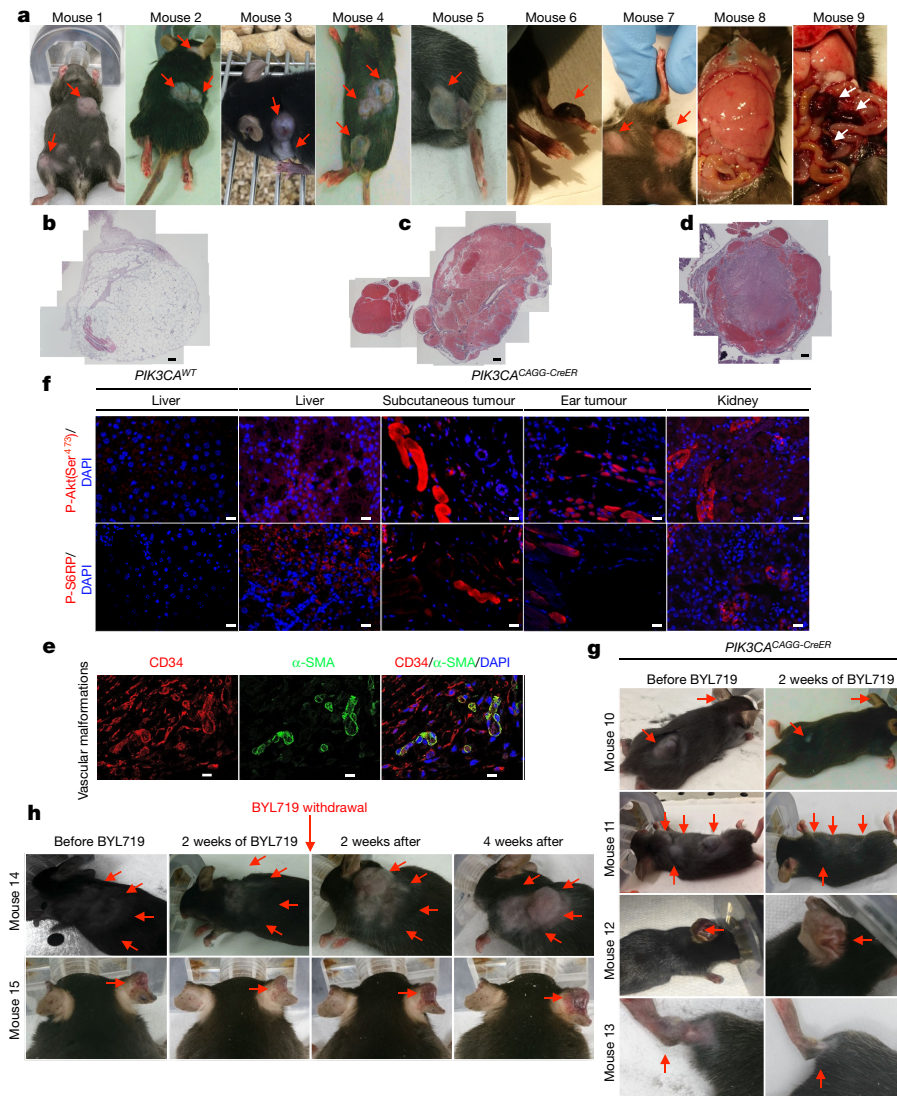


Fig. 2 | Characterization of the second mouse model of PROS and efficacy of BYL719. **a**, Morphology of $PIK3CA^{CAGG-CreER}$ mice one month after *Cre* induction with a single dose of 4 mg kg^{-1} tamoxifen. The mice displayed multiple visible deforming tumours across the whole body (red arrows). Some of these tumours had huge vascular irregularities. The mice progressively developed hypertrophic extremities, enlarged liver with aberrant vessels, and multiple intraabdominal vascular malformations (pictures representative of nine mice). **b–d**, Histopathological examination of the tumours revealed the presence of lipomatous tumours (**b**; $n = 10$ mice examined) and multiple venous malformations composed of ecstatic venous channels with a thin endothelial cell lining, surrounded by sparse, erratically distributed vascular smooth muscle cells and a disorganized extracellular matrix (**c**, **d**; $n = 10$ mice examined). Scale bars, $50\ \mu\text{m}$. **e**, Coimmunostaining of CD34 and α -smooth muscle cells in venous malformation ($n = 10$ mice examined). **f**, Immunofluorescence staining

for P-AKT (Ser⁴⁷³) and P-S6RP in the liver, subcutaneous tumour, ear tumour and kidneys of $PIK3CA^{WT}$ and $PIK3CA^{CAGG-CreER}$ mice ($n = 10$ mice examined per group). Scale bars, $10\ \mu\text{m}$. **g**, $PIK3CA^{CAGG-CreER}$ mice were injected with a single dose of 4 mg kg^{-1} tamoxifen and followed for one month after *Cre* induction. Once the tumours reached a certain volume, the mice were treated with BYL719 for two weeks and this led to the disappearance of all tumours ($n = 18$ mice). **h**, $PIK3CA^{CAGG-CreER}$ mice were injected with a single dose of 4 mg kg^{-1} tamoxifen and followed for one month after *Cre* induction. Once the tumours reached a certain volume, the mice were treated with BYL719 for two weeks and this led to the disappearance of all tumours ($n = 7$ mice). Then, BYL719 treatment was withdrawal and we observed the recurrence of tumours and vascular malformations in $PIK3CA^{CAGG-CreER}$ mice within the next four weeks.

observed a marked improvement in skin hypertrophy, with a change in nevus coloration and a reduction in ear size (Fig. 3a). Finally, after 6 months of BYL719 treatment, the patient began to partially gain bladder function, with an improvement in saddle anaesthesia. MRI revealed a 60% reduction in the size of the venous malformation that was compressing his spinal cord. The patient's Karnofsky and ECOG scores increased to 80% and 1, respectively. After eighteen months of treatment, the patient had no side effects except hyperglycaemia which was well controlled with nutrition therapy. BYL719 leads to peripheral insulin resistance¹¹ and hyperglycaemia was one of the most common drug-related adverse events in the phase I trial¹². The patient is currently still under BYL719 treatment.

Patient 2 was a nine-year-old girl with a PROS/CLOVES syndrome diagnosed two years before this study and a gain of function $PIK3CA\ c.3140A > G$ (H1047R) mosaicism mutation (12% mosaicism) confirmed by skin biopsy. She had scoliosis, left leg hypertrophy, vascular malformations, and hypertrophic back muscles (Fig. 4a). She also had a voluminous cystic lymphangioma involving the left kidney and the gastrointestinal tract. A PET scan showed metabolic fixation in the thymus, back muscles, and left leg muscles (Fig. 4d). Her Karnofsky and ECOG scores were 50% and 3, respectively. BYL719 was started at the lowest available dosage: 50 mg per day. As in the first patient, we observed a marked clinical improvement rapidly after the onset of treatment (Fig. 4a). The patient reported improved comfort and we observed a

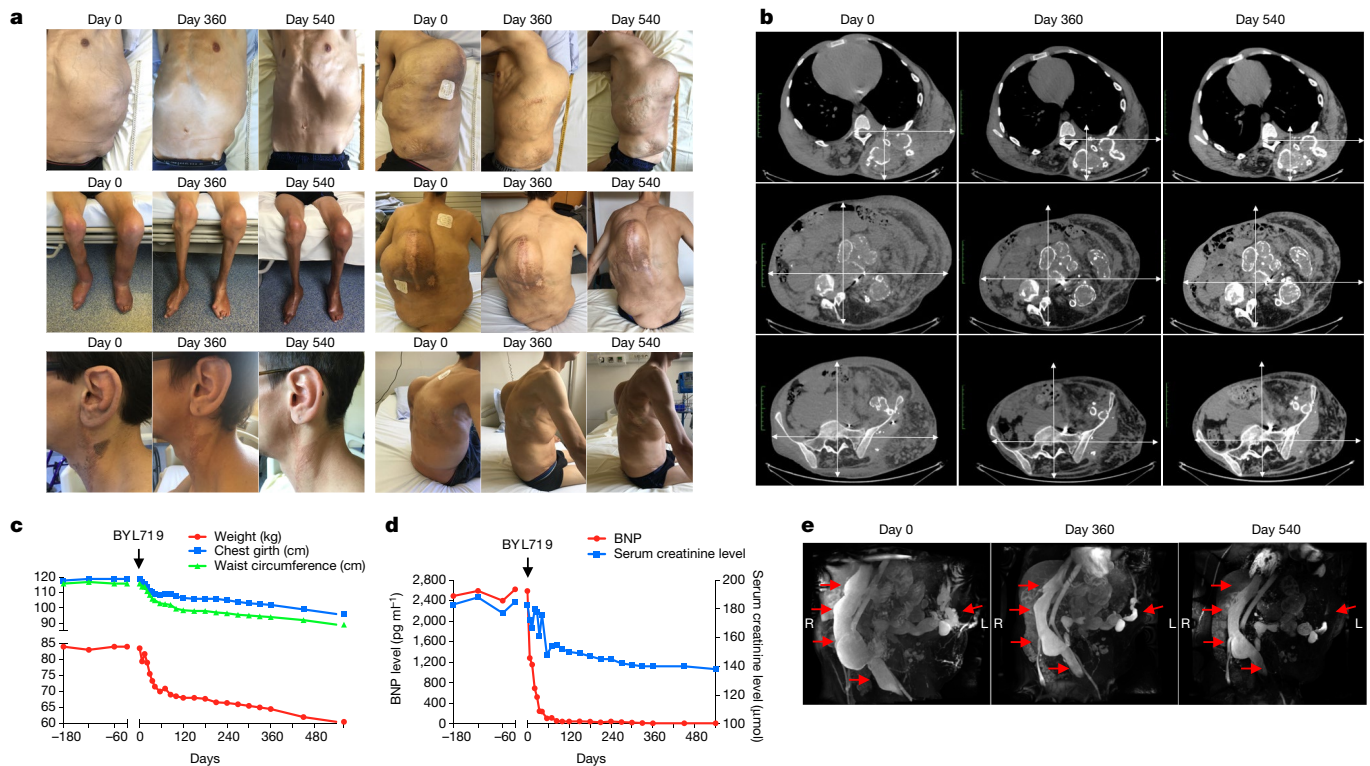


Fig. 3 | Efficacy of BYL719 treatment in an adult patient with severe CLOVES syndrome. **a**, Representative pictures of patient 1 before and 360 and 540 days after onset of BYL719 treatment. **b**, CT scans of patient 1 before and 360 and 540 days after onset of BYL719 treatment. The magnifications are the same. **c**, Clinical parameters (weight, chest girth and waist circumference) of patient 1 before and after onset of BYL719

treatment. **d**, Serum BNP and creatinine levels before and after onset of BYL719 treatment. **e**, Three-dimensional MRI-based reconstructions of the intra-abdominal vessels before and after onset of BYL719 treatment. The total volume of the venous malformation was reduced by up to 72% after 540 days of treatment.

24% reduction in her left leg volume, reduced left foot volume, and a 14% reduction in her abdominal circumference (Fig. 4b) after 12 months. The hypertrophic muscles in her back also shrank rapidly and, unexpectedly, her scoliosis was reversed after 6 months without any other intervention (Fig. 4c). More importantly, MRI showed a 40%, 54% and 71%

reduction in intra-abdominal tumour volume after 4, 6 and 12 months of treatment, respectively (Fig. 4e). A PET scan performed at the same time points confirmed the marked reduction in metabolic activity of the affected tissues (Fig. 4d). The patient's Karnofsky and ECOG scores were greatly improved, to 100% and 0, respectively. Her height had increased

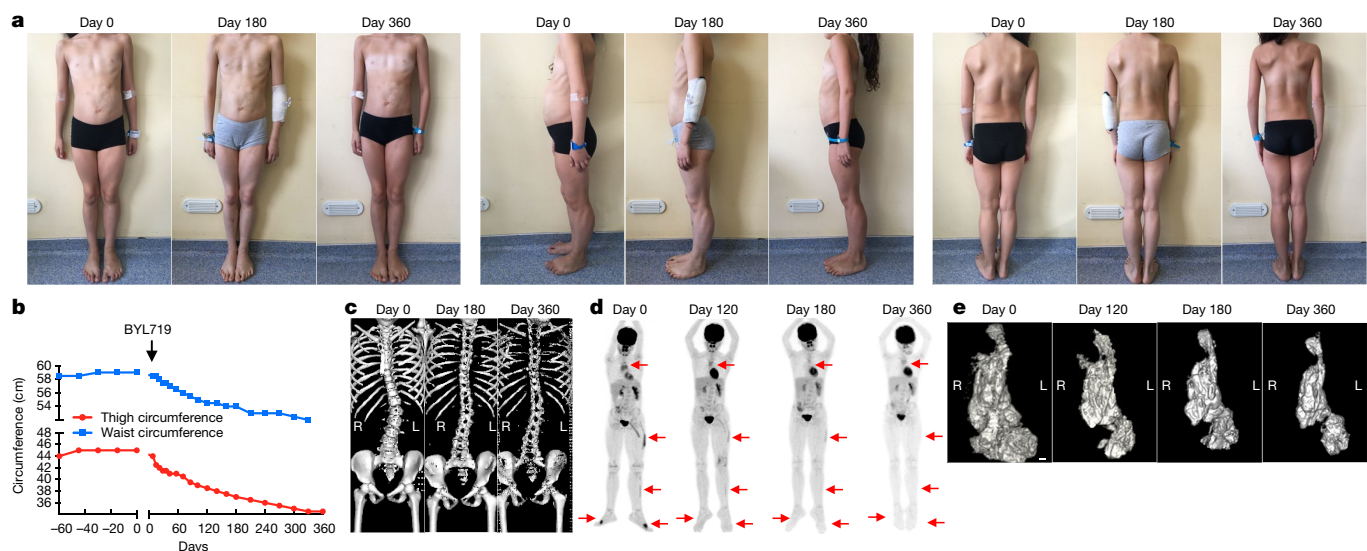


Fig. 4 | Efficacy of BYL719 treatment in a child patient with severe CLOVES syndrome. **a**, Representative pictures of patient 2 before and 180 and 360 days after onset of BYL719 treatment. **b**, Clinical parameters (thigh and waist circumferences) of patient 2 before and after onset of BYL719 treatment. **c**, Three-dimensional CT scan reconstruction of the spine before and 180 and 360 days after onset of BYL719 treatment.

d, PET scan images of patient 2 before and 120, 180 and 360 days after onset of BYL719 treatment. Arrows indicate the hypermetabolic tissues before and during treatment. **e**, Three-dimensional MRI-based reconstruction of the intra-abdominal tumour before and 120, 180 and 360 days after onset of BYL719 treatment. The tumour volume was reduced by up to 71% after 360 days of treatment. Scale bar, 1 cm.



Fig. 5 | Efficacy of BYL719 treatment in patients with PROS. Images of patients 1–9 before and after six months of BYL719 treatment. Patient 1 is a four-year-old girl suffering from severe vascular malformations involving the right arm and chest with permanent pain. After six months of treatment we saw a marked improvement in all vascular malformations as well as the scoliosis. Patient 2 is a 4-year-old girl with scoliosis and hypertrophic left buttock who had already undergone left foot partial amputation. After six months of treatment we saw an improvement in the scoliosis and reduction of the hypertrophic lesion. Patient 3 is a 5-year-old girl with CLOVES syndrome and chronic gastrointestinal bleeding. After six months of treatment, chronic bleeding stopped. Patient 4 is a 5-year-old girl with left hemifacial hyperplasia that was progressing despite multiple surgeries. After six months of treatment we saw for the first time an improvement in the hypertrophy (not shown for reasons of

confidentiality). Patient 5 is a 6-year-old boy with CLOVES syndrome. The treatment led to a reduction in lipomatous tumours and scoliosis. Patient 6 is a 10-year-old girl with CLOVES syndrome and a severe lipomatous tumour on her back. BYL719 led to a marked improvement in the scoliosis and shrinkage of the tumour. Patient 7 is an 11-year-old boy with CLOVES syndrome, chronic gastrointestinal bleeding and severe dyspnea. Treatment improved all symptoms and the bleeding stopped. Patient 8 is an 11-year-old girl with CLOVES syndrome and severe dyspnea. Treatment improved the subcutaneous lipoma as well as dyspnea. Patient 9 is a 13-year-old girl with CLOVES syndrome, splenomegaly and severe vascular malformations involving the left kidney and limbs. Vascular malformations were markedly improved and the size of the spleen reduced after treatment.

by 0.6 cm per month during the 6 months before BYL719 treatment began, and growth remained stable at 0.6 cm per month during the 12-month treatment period. Her glycaemia remained normal and her glycated haemoglobin (HbA1c) level, which was 5.5% before BYL719 treatment, was 5.1, 4.9 and 5.0% after 3, 6 and 12 months of treatment, respectively. The patient is still receiving BYL719 treatment.

BYL719 in a cohort of PROS patients

On the basis of these results, we were authorized to administer BYL719 to 17 additional patients with PROS who had life-threatening complications and/or were scheduled for debulking surgery (Fig. 5 and Extended Data Fig. 11a). The demographical characteristics of the patients are listed in Supplementary Table 1. All patients had documented gain-of-function mutations in the *PIK3CA* gene, with ten different mutations (Extended Data Fig. 11b and Supplementary Table 1). All patients underwent clinical examination, laboratory evaluation, PET and MRI scans before BYL719 administration and 3 and 6 months after. Fourteen children were started at the lowest available dosage, 50 mg per day and three adults at 250 mg per day. Among the 17 patients, six had been diagnosed with CLOVES syndrome, two with megalencephaly–capillary malformation (MCAP), and nine with localized overgrowth syndrome (back, limbs, face, arms) including three patients with abdominal or chest vascular tumours. In addition, each patient had peculiar clinical features, and twelve patients had undergone previous debulking surgery (Fig. 5 and Extended Data Fig. 11a). Eight patients had received previous rapamycin treatment for 18 months without clinical or radiological improvement.

After BYL719, all patients showed substantial clinical improvement (Supplementary Table 1). All patients described reduced

tiredness. The mean circumference of the clinical target lesions decreased by 12.6 ± 3.8 and $16.3 \pm 3.9\%$ after 3 and 6 months of BYL719 treatment, respectively (Supplementary Table 2 and Extended Data Fig. 11c). All patients demonstrated an improvement in skin capillary abnormalities and naevi became thinner. The two opioid-dependent patients who were confined to bed could stop morphine, and after 2 months of treatment were able to walk without help; tiredness improved, and haematuria disappeared in patient 11. Chronic gastrointestinal bleeding stopped in three patients, associated with the correction of disseminated intravascular coagulation in patients 7 and 9, which led to the cessation of heparin treatment. We also observed an improvement in chronic palpebral cellulitis in patient 14 and we were able to progressively taper down this patient's steroid treatment. All patients demonstrated a clinical improvement in scoliosis and the surgical corset was removed from patient 6. In the two patients with MCAP (patients 13 and 14), we observed an improvement in cognitive function and behaviour. After 6 months of treatment, all patients were still alive and no surgery had been performed.

Introduction of BYL719 initially led to weight loss with a maximum after two months of treatment ($-1.7 \pm 3.1\%$). However, after five months of treatment, body weight came back to baseline and patients started to gain weight (Extended Data Fig. 11d). Notably, four obese patients showed a marked reduction in body weight ($-9.7 \pm 8.2\%$; Extended Data Fig. 11e). This reduction was not associated with a reduction in food intake. MRI demonstrated a notable reduction in subcutaneous fat in these patients. The growth of the children⁴ was not affected by the drug during the six months of treatment (Extended Data Fig. 12a).

In addition to the clinical improvement, we observed a radiological response in all patients. After 90 and 180 days of therapy, the mean volume of the target lesions had decreased by 27.2 ± 14.6 and $37.8 \pm 16.3\%$, respectively (Extended Data Fig. 12b–e). All target lesions responded to treatment. Notably, in the two patients with MCAP, MRI revealed an improvement in cerebral perfusion (Extended Data Fig. 12f). Finally, 5 of the 17 patients had hypermetabolic activity as assessed by PET scan. Remarkably, after 90 days of treatment we observed a drastic reduction in the metabolic activity of affected tissues (Extended Data Fig. 12g).

Although our follow-up period was short, we observed a low rate of side effects using this drug. Indeed, we noticed only discrete mouth ulcerations in three patients during one week that disappeared spontaneously (grade I). BYL719 was not associated with organ toxicity during this period (as assessed by heart, liver, kidney function and blood testing). Transient hyperglycaemia occurred in one obese patient (patient 15). Hyperglycaemia was well controlled with diet restriction only. Patient 17 was diabetic before BYL719 introduction and needed to increase the posology of oral antidiabetic drugs. Glycated haemoglobin remained normal during treatment in all patients (data not shown). All of the patients are still receiving BYL719 treatment.

Discussion

We have described a mouse model of PROS/CLOVES that mimics elements of the human phenotype by allowing titration of mosaicism; we have shown that BYL719 treatment rescues the PROS phenotype in the mouse model more efficaciously than rapamycin; and we have demonstrated that BYL719 is clinically effective, with a promising safety profile, in patients with PROS regardless of the type of *PIK3CA* mutation. This study provides the first direct evidence that *PIK3CA* inhibition is a robust and effective therapeutic strategy that can markedly improve the outcome of PROS patients.

Online content

Any Methods, including any statements of data availability and Nature Research reporting summaries, along with any additional references and Source Data files, are available in the online version of the paper at <https://doi.org/10.1038/s41586-018-0217-9>.

Received: 1 March 2017; Accepted: 16 May 2018;

Published online 13 June 2018.

1. Vanhaesebroeck, B., Stephens, L. & Hawkins, P. PI3K signalling: the path to discovery and understanding. *Nat. Rev. Mol. Cell Biol.* **13**, 195–203 (2012).
2. Hiles, I. D. et al. Phosphatidylinositol 3-kinase: structure and expression of the 110 kd catalytic subunit. *Cell* **70**, 419–429 (1992).
3. Stephens, L. et al. Protein kinase B kinases that mediate phosphatidylinositol 3,4,5-trisphosphate-dependent activation of protein kinase B. *Science* **279**, 710–714 (1998).
4. Manning, B. D. & Toker, A. AKT/PKB signaling: navigating the network. *Cell* **169**, 381–405 (2017).
5. Keppler-Noreuil, K. M. et al. *PIK3CA*-related overgrowth spectrum (PROS): diagnostic and testing eligibility criteria, differential diagnosis, and evaluation. *Am. J. Med. Genet. A.* **167A**, 287–295 (2015).
6. Keppler-Noreuil, K. M. et al. Clinical delineation and natural history of the *PIK3CA*-related overgrowth spectrum. *Am. J. Med. Genet. A.* **164A**, 1713–1733 (2014).
7. Kurek, K. C. et al. Somatic mosaic activating mutations in *PIK3CA* cause CLOVES syndrome. *Am. J. Hum. Genet.* **90**, 1108–1115 (2012).
8. Canaud, G. et al. *AKT2* is essential to maintain podocyte viability and function during chronic kidney disease. *Nat. Med.* **19**, 1288–1296 (2013).
9. Engelman, J. A. Targeting PI3K signalling in cancer: opportunities, challenges and limitations. *Nat. Rev. Cancer* **9**, 550–562 (2009).
10. Furet, P. et al. Discovery of NVP-BYL719 a potent and selective phosphatidylinositol-3 kinase alpha inhibitor selected for clinical evaluation. *Bioorg. Med. Chem. Lett.* **23**, 3741–3748 (2013).
11. Fritsch, C. et al. Characterization of the novel and specific $PI3K\alpha$ inhibitor NVP-BYL719 and development of the patient stratification strategy for clinical trials. *Mol. Cancer Ther.* **13**, 1117–1129 (2014).

12. Mayer, I. A. et al. A phase Ib study of alpelisib (BYL719), a $PI3K\alpha$ -specific inhibitor, with letrozole in ER+/HER2– metastatic breast cancer. *Clin. Cancer Res.* **23**, 26–34 (2017).
13. Srinivasan, L. et al. PI3 kinase signals BCR-dependent mature B cell survival. *Cell* **139**, 573–586 (2009).
14. Klippel, A. et al. Membrane localization of phosphatidylinositol 3-kinase is sufficient to activate multiple signal-transducing kinase pathways. *Mol. Cell Biol.* **16**, 4117–4127 (1996).
15. Hayashi, S. & McMahon, A. P. Efficient recombination in diverse tissues by a tamoxifen-inducible form of Cre: a tool for temporally regulated gene activation/inactivation in the mouse. *Dev. Biol.* **244**, 305–318 (2002).
16. Castillo, S. D. et al. Somatic activating mutations in *Pik3ca* cause sporadic venous malformations in mice and humans. *Sci. Transl. Med.* **8**, 332ra43 (2016).
17. Hare, L. M. et al. Heterozygous expression of the oncogenic *Pik3ca*(H1047R) mutation during murine development results in fatal embryonic and extraembryonic defects. *Dev. Biol.* **404**, 14–26 (2015).
18. Mirzaa, G. et al. *PIK3CA*-associated developmental disorders exhibit distinct classes of mutations with variable expression and tissue distribution. *JCI Insight* **1**, e87623 (2016).
19. Kinross, K. M. et al. Ubiquitous expression of the *Pik3ca*H1047R mutation promotes hypoglycemia, hypoinsulinemia, and organomegaly. *FASEB J.* **29**, 1426–1434 (2015).
20. Hammill, A. M. et al. Sirolimus for the treatment of complicated vascular anomalies in children. *Pediatr. Blood Cancer* **57**, 1018–1024 (2011).
21. O'Reilly, K. E. et al. mTOR inhibition induces upstream receptor tyrosine kinase signaling and activates Akt. *Cancer Res.* **66**, 1500–1508 (2006).
22. Heitman, J., Movva, N. R. & Hall, M. N. Targets for cell cycle arrest by the immunosuppressant rapamycin in yeast. *Science* **253**, 905–909 (1991).
23. Velarde-Jurado, E. & Avila-Figueroa, C. [Evaluation of the quality of life]. *Salud Publica Mex.* **44**, 349–361 (2002).
24. Oken, M. M. et al. Toxicity and response criteria of the Eastern Cooperative Oncology Group. *Am. J. Clin. Oncol.* **5**, 649–655 (1982).

Acknowledgements This project received funding from the European Research Council under the European Union's Horizon 2020 research and innovation program grants, (STG-2015) 679254 and (PoC-2016) 737546 (both awarded to G.C.). This work was also supported by the Emmanuel BOUSSARD Foundation, the DAY SOLVAY Foundation, Fondation TOURRE, Fondation Simone et Cino Del Duca, INSERM, Assistance Publique—Hôpitaux de Paris and the University of Paris, Descartes. We would like to thank the two patients and their families. We also thank C. Semaille from the ANSM for help and advice; S. Bisot-Locard (Novartis) for the BYL719; G. Autret for performing the mouse MRIs; S. Berissi and colleagues at the Plateforme d'histologie et morphologie du petit animal, INEM, Paris; S. Principe for administrative management; A. Klippel for advice and for providing plasmids encoding *Myr-p110*myc* and *Myr-p110*KR-myc* constructs; K. Rajewsky for advice; and the radiological team from the Centre d'Imagerie de Franconville and in particular M. Canaud and A. Scemama for their help.

Reviewer information Nature thanks E. Baselga, W. Dobyns, R. Semple and B. Vanhaesebroeck for their contribution to the peer review of this work.

Author contributions Q.V. performed the experiments and analysed the data. T.B., S.H.R., O.B., S.S., S.P., F.M., B.K., P.M., N.G., D.J., V.C.-D., C.M., A.P., S.C.J., V.S., S.Ly., C.L.-R., L.G., C.B., J.A. and C.L. followed the patients and analysed the data. L.B. and N.B. performed the patient CT scans and MRIs and analysed the data. E.B. performed the PET scans and analysed the data. S.La., S.M., J.Y. and S.C.J. performed some in vivo and in vitro experiments. C.H. performed some mouse experiments. J.-P.D. analysed all the histological findings. C.B.-F performed *PIK3CA* genotyping in patients. J.S., L.S. and C.C. performed and analysed the mouse CT scans. F.T. was involved in data analysis and helped to write the paper. G.C. followed the patients, provided the conceptual framework, designed the study, supervised the project, and wrote the paper.

Competing interests A patent application (WO2017140828A1) has been filed by INSERM (Institut National de la Santé et de la Recherche Médicale), Centre National De La Recherche Scientifique (CNRS), Université Paris Descartes, and Assistance Publique-Hôpitaux De Paris (AP-HP) for the use of BYL719 (alpelisib) in the treatment of *PIK3CA*-related overgrowth spectrum (PROS/CLOVES syndrome). G.C. is the inventor.

Additional information

Extended data is available for this paper at <https://doi.org/10.1038/s41586-018-0217-9>.

Supplementary information is available for this paper at <https://doi.org/10.1038/s41586-018-0217-9>.

Reprints and permissions information is available at <http://www.nature.com/reprints>.

Correspondence and requests for materials should be addressed to G.C.

Publisher's note: Springer Nature remains neutral with regard to jurisdictional claims in published maps and institutional affiliations.

METHODS

Mice. For this study, we interbred homozygous *R26Stop^{FL}P110** (Stock# 012343) and heterozygous *CAGGCre-ERTM* (Stock# 004682) mice on the C57BL/6 background obtained from Jackson Laboratories. We obtained *R26Stop^{FL}P110*^{+/-}* × *CAGGCre-ERTM* mice (referred to here as *PIK3CA^{CAGG-CreER}* mice) and *R26Stop^{FL}P110*^{+/+}* × *CAGGCre-ERTM* mice (referred to here as *PIK3CA^{WT}* mice). We used the p110* construct¹⁴ (Extended Data Fig. 9). The p110* protein is a constitutively active chimera that contains the iSH2 domain of p85 fused to the N terminus of p110 via a flexible glycine-linker. To generate tissue-specific p110*-transgenic mice, a cloned loxP-flanked neoR-stop cassette was inserted into a modified version of pROSA26-1 followed by the cDNA encoding p110* and then a frt-flanked IRES-EGFP cassette and a bovine polyadenylation sequence (*R26StopFLP110**)¹³.

No statistical methods were used to predetermine sample size. The experiments were not randomized and the investigators were not blinded to allocation during experiments and outcome assessment.

Animals were fed ad libitum and housed at a constant ambient temperature in a 12-h light cycle. Animal procedures were approved by the 'Services Vétérinaires de la Préfecture de Police de Paris' Departmental Director and by the ethical committee of the Paris Descartes University. All appropriate procedures were followed to ensure animal welfare. In the first study, a single dose of tamoxifen (40 mg kg⁻¹) was administered by oral gavage when the mice were 21 days old. For the survival studies, the mice were followed daily after tamoxifen gavage (*PIK3CA^{WT}* *n* = 16 and *PIK3CA^{CAGG-CreER}* *n* = 16). For the preventive studies, the mice were treated with BYL719 (MedChem Express; 50 mg kg⁻¹ in 0.5% carboxymethylcellulose (Sigma Aldrich), daily p.o.) (*n* = 16) or vehicle (0.5% carboxymethylcellulose (Sigma Aldrich), daily p.o.) (*n* = 16). For the therapeutic studies, the mice were treated with BYL719 (50 mg kg⁻¹ in 0.5% carboxymethylcellulose (Sigma Aldrich), daily p.o.) (*n* = 12) or vehicle (0.5% carboxymethylcellulose (Sigma Aldrich), daily p.o.) (*n* = 12). Treatment was started at the time of tamoxifen gavage for the preventive study, or seven days later for the therapeutic study.

In the second study, a single dose of tamoxifen (4 mg kg⁻¹) was administered by oral gavage when the mice were 21 days old (*PIK3CA^{CAGG-CreER}* *n* = 28). Ten mice were killed at approximately 1 month after tamoxifen gavage when tumours reached a certain volume, for tissue examination. Once gross morphological abnormalities were visible, eighteen mice were treated with BYL719 for 15 days and treatment was stopped once macroscopic lesions disappeared to follow their phenotype.

In the third study, a single dose of tamoxifen (40 mg kg⁻¹) was administered through oral gavage when the mice were 21 days old and the mice were then treated with daily intraperitoneal injection of rapamycin (MedChem Express, ref#HY-10219) (*PIK3CA^{CAGG-CreER}* *n* = 7) or vehicle (*PIK3CA^{CAGG-CreER}* *n* = 7) for 30 days. Rapamycin was dissolved to a final concentration of 0.5 mg ml⁻¹ in absolute ethanol dissolved further in 5% polyethylene glycol (PEG-400) and 5% Tween 80 in PBS and used for intraperitoneal injection at 4 mg kg⁻¹. All mice treated with rapamycin or vehicle were then killed for tissue examination.

In the fourth study, a single dose of tamoxifen (4 mg kg⁻¹) was administered by oral gavage when the mice were at 21 days old (*PIK3CA^{CAGG-CreER}* *n* = 6). Once gross morphological abnormalities were visible (approximately 30 days later), all the mice were treated with daily intraperitoneal injection of rapamycin (MedChem Express, ref#HY-10219) for 30 days. Rapamycin was dissolved to a final concentration of 0.5 mg ml⁻¹ in absolute ethanol dissolved further in 5% polyethylene glycol (PEG-400) and 5% Tween 80 in PBS and used for intraperitoneal injection at 4 mg kg⁻¹.

Cell cultures, plasmids and transfection. HeLa cells were grown at 37 °C in Dulbecco's modified Eagle's medium (DMEM) containing 10% fetal bovine serum (Sigma). Transient transfections were performed with cDNAs encoding wild-type *PIK3CA* (Addgene Inc., ID 16643), *PIK3CA* (Exon20 H1047R) (Addgene Inc., ID 16639) and *PIK3CA* (Exon9 E545K) (Addgene Inc., ID 16642) constructs and *Myr-p110*-myc* and *Myr-p110*KR-myc* constructs¹⁴ using the Lipofectamine 2000 transfection reagent following the manufacturer's instructions. Cells were lysed in RIPA buffer for protein extraction 48 h after transfection and 12 h after starvation. Each experiment was performed in duplicate and repeated at least four times.

Skin samples were collected from the *PIK3CA^{WT}* and *PIK3CA^{CAGG-CreER}* mice using standard methods²⁵. To generate dermal fibroblast cultures, skin samples were minced and incubated at room temperature in 0.05% trypsin-EDTA (ThermoFisher) solution for 30 min with gentle shaking. Cells were collected by centrifuging at 700g for 10 min, resuspended in cell culture medium containing 25% FBS, and plated onto 24-well plates to establish lines. Fibroblast cultures were grown and maintained in 1 × MEM (Corning) supplemented with 25% FBS and penicillin/streptomycin (Corning) to a final concentration of 100 IU penicillin and 500 µg ml⁻¹ streptomycin.

Cells at similar population doubling were plated 1:4 from confluent cultures and allowed to grow until ~80% confluent. Then, medium was replaced with

medium containing 4-OH tamoxifen (1 µM) (Sigma) for 48 h to activate the *Cre* recombinase. Cells were then starved for 12 h and exposed for 24 h to either BYL719 (0.1 or 1.0 µmol l⁻¹; MedChem Express) or rapamycin (10 or 100 ng ml⁻¹; Sigma) or an equal volume of DMSO. Cells were rinsed with 1 × PBS. Protein lysates were collected by directly adding 1 × RIPA buffer containing protease and phosphatase inhibitors. Each experiment was performed in duplicate and repeated at least four times.

Morphological analysis. Mouse tissues were fixed in 4% paraformaldehyde and paraffin embedded. 4-µm liver sections were stained with periodic acid-Schiff (PAS), 4-µm liver or spleen sections were stained with haematoxylin and eosin (HE), and 4-µm kidney sections were stained with Masson's trichrome. Four-µm liver frozen sections were stained with Oil red O (Sigma Aldrich, ref# 00625).

Immunohistochemistry and immunofluorescence. Paraffin-embedded kidney sections (4 µm) were incubated with anti-P-AKT (Ser⁴⁷³) antibody (Cell Signaling Technology, ref#4051 dilution 1:100), anti-P-S6RP antibody (Cell Signaling Technology, ref# 5364, dilution 1:100), anti-α-smooth muscle cell antibody (Sigma Aldrich, ref# A5228, dilution 1:100), anti-CD34 antibody (eBioscience, ref# 14-0341, dilution 1:100), anti-CD31 antibody (Dianova, ref# Dia-310, dilution 1:30) or anti-podoplanin antibody (Agilent, ref#M3619, dilution 1:50). Immunofluorescence studies were analysed using a Zeiss LSM 700 confocal microscope.

Proliferation assay. Proliferative cells were detected in tissues using Ki67 immunostaining (anti-Ki67 antibody, Thermo Fisher Scientific, ref# RM-9106-S1, dilution 1:100). 4-µm kidney sections were incubated with anti-Ki67 antibody, followed by a biotinylated mouse antibody (Vector) at 1:400 and a HRP-labelled streptavidin at 1:1,000. Staining was revealed by DAB. The proliferation index (PI) per tissue was calculated as the number of Ki67-positive nuclei for the total number of nuclei in 10 randomly selected fields (magnification × 400).

Apoptosis assay. Apoptosis was detected in 4-µm sections of paraffin-embedded tissues (liver, spleen and heart) by TUNEL assay using the in situ Cell Death Detection kit (Roche) according to the manufacturer's protocol. The number of apoptotic cells was determined as the number of TUNEL-positive nuclei per field in 10 randomly selected fields (magnification × 400).

β-galactosidase. Fresh tissues were briefly rinsed in PBS and then washed three times in PBS containing 5 mM EGTA, 2 mM MgCl₂, 0.02% nonidet and 0.01% Na desoxycholate. Samples were rinsed in PBS and then fixed in 20% formaldehyde/2% glutaraldehyde for 45 min. Tissues were then immersed overnight in β-galactosidase staining solution. After rinsing in PBS, livers were fixed in 4% formaldehyde and paraffin embedded. 4-µm tissue sections were counterstained with haematoxylin and eosin. We then counted the number of cells with β-galactosidase staining per field in 10 randomly selected fields (magnification × 400).

mRNA analysis. mRNAs were quantified in mouse tissues by quantitative PCR with reverse transcriptase (RT-PCR) using an ABI PRISM 7700 Sequence Detection system (Applied Biosystems). Primers were as follows: p16 (fwd) 5'-GGCCAATCCCAAGAGCAGAG-3' and (rev) 5'-GC CACATGCTAGACACGCTA-3'; RPL13 (fwd) 5'-CTCATCCTGTTCCC CAGGAA-3' and (rev) 5'-GGGTGGCCAGCTTAAGTTCTT-3'. RPL13 was used as the normalization control as previously described²⁶.

Western blot. Western blots were performed as previously described²⁷. In brief, protein extracts from the liver, muscles, heart, kidneys and fibroblasts were resolved by SDS-PAGE before being transferred onto the appropriate membrane and incubated with anti-P-AKT (Ser⁴⁷³) antibody (Cell Signaling Technology, ref# 4060, dilution 1:1,000), anti-P-AKT (Thr³⁰⁸) antibody (Cell Signaling Technology, ref# 13038, dilution 1:1,000), anti-AKT antibody (Cell Signaling Technology, ref# 9272, dilution 1:1,000), anti-P-S6RP antibody (Cell Signaling Technology, ref# 5364, dilution 1:1,000), anti-p110α (Cell Signaling Technology, ref# 4249, dilution 1:1,000), anti-LYVE-1 (R&D Systems, ref# AF2125, dilution 1:1,000), anti-P-p44/42 antibody (Cell Signaling Technology, ref# 4370, dilution 1:1,000), anti-p44/42 (Thr²⁰²/Tyr²⁰⁴) antibody (Cell Signaling Technology, ref# 9102, dilution 1:1,000), anti-P-p38 (Thr¹⁸⁰/Tyr¹⁸²) antibody (Cell Signaling Technology, ref# 9216, dilution 1:1,000), anti-p38 antibody (Cell Signaling Technology, ref# 8690, dilution 1:1,000), anti-GFP antibody (Abcam, ref# ab13970, dilution 1:1,000), anti-GAPDH (Merck Millipore, ref#374, dilution 1:1,000) or anti-β-actin antibody (Sigma-Aldrich, ref#A2228, dilution 1:1,000), followed by the appropriate peroxidase-conjugated secondary antibody (dilution 1:10,000). Chemiluminescence was acquired using a Fusion FX7 camera (Vilbert Lourmat) and densitometry was performed using the Bio1D software (Certain Tech).

CT scan and MRI evaluation. High resolution micro-CT scans were performed at the Plateforme PIV, EA2496—Pathologie, Imagerie et Biothérapies orofaciales, Dental school Paris V. In brief, 4-week-old female *PIK3CA^{WT}* and *PIK3CA^{CAGG-CreER}* mice induced with 40 mg kg⁻¹ tamoxifen received either vehicle (*n* = 3 *PIK3CA^{WT}* mice) or BYL719 (*n* = 3 *PIK3CA^{WT}* mice, *n* = 3 *PIK3CA^{CAGG-CreER}* mice) for 14 days. Additionally, *PIK3CA^{CAGG-CreER}* mice (*n* = 3 mice) received

a single dose of 4 mg kg⁻¹ tamoxifen one month earlier in order to induce the development of tumours and hypertrophic extremities. High-resolution micro-CT scans were performed under general anaesthesia before treatment and 7 and 14 days later.

MRI scans were performed at the Plateforme IRM, INSERM U970, Centre de recherche cardiovasculaire de Paris. In brief, MRI scans were performed under general anaesthesia in 4-week-old female *PIK3CA*^{WT} ($n=6$) and *PIK3CA*^{CAGG-CreER} ($n=6$) mice 7 days after they received a single dose of 40 mg kg⁻¹ tamoxifen to induce *Cre* recombination. MRI scans were then repeated weekly in all mice for 1 month.

Flow cytometry. Spleens of *PIK3CA*^{WT} ($n=12$) mice, *PIK3CA*^{CAGG-CreER} mice induced with 40 mg kg⁻¹ tamoxifen ($n=6$) and *PIK3CA*^{CAGG-CreER} mice induced with 4 mg kg⁻¹ tamoxifen ($n=6$) were mechanically disrupted in PBS/SVF 2%. Following dissociation, spleens were filtered, centrifuged and resuspended. Cells were then treated with an FC blocker for 10 min at 4 °C (Biolegend, ref# 101302) and fixed/permeabilized (BD Bioscience, ref# 554714). Cells were labelled with chicken polyclonal anti-GFP antibody (Abcam, ref# ab13970) for 30 min at 4 °C. Subsequently, cells were incubated with Alexa Fluor 647-labelled goat anti-chicken IgY antibody (Abcam, ref# ab150171) for 30 min at 4 °C. A background control incubated only with secondary antibody was also included. Samples were analysed using Gallios Flow Cytometer (Beckman Coulter) and FlowJo software (TreeStar). The mosaicism was assessed by the ratio of the number of GFP-positive cells to the total number of cells.

Patients. The study was conducted on 19 patients (4 adults and 15 children) followed at Necker hospital. This protocol was approved by the 'Agence Nationale de Sécurité du Médicament et des Produits de Santé' (ANSM, authorizations n°: 553984–553986, 584018, 585881–586135, 585464, 585465, 585467, 585880, 586136, 585463, 596229, 588018, 587904, 587896–587912, 587908, 587905, 587910, 585458, 595374 and 587899) and informed written consent was obtained from the adult patients and the legal representatives of the children. BYL719 was compassionately offered by Novartis. Adult patients received 250 mg per day and child patients received 50 mg per day. BYL719 was taken orally every morning before breakfast.

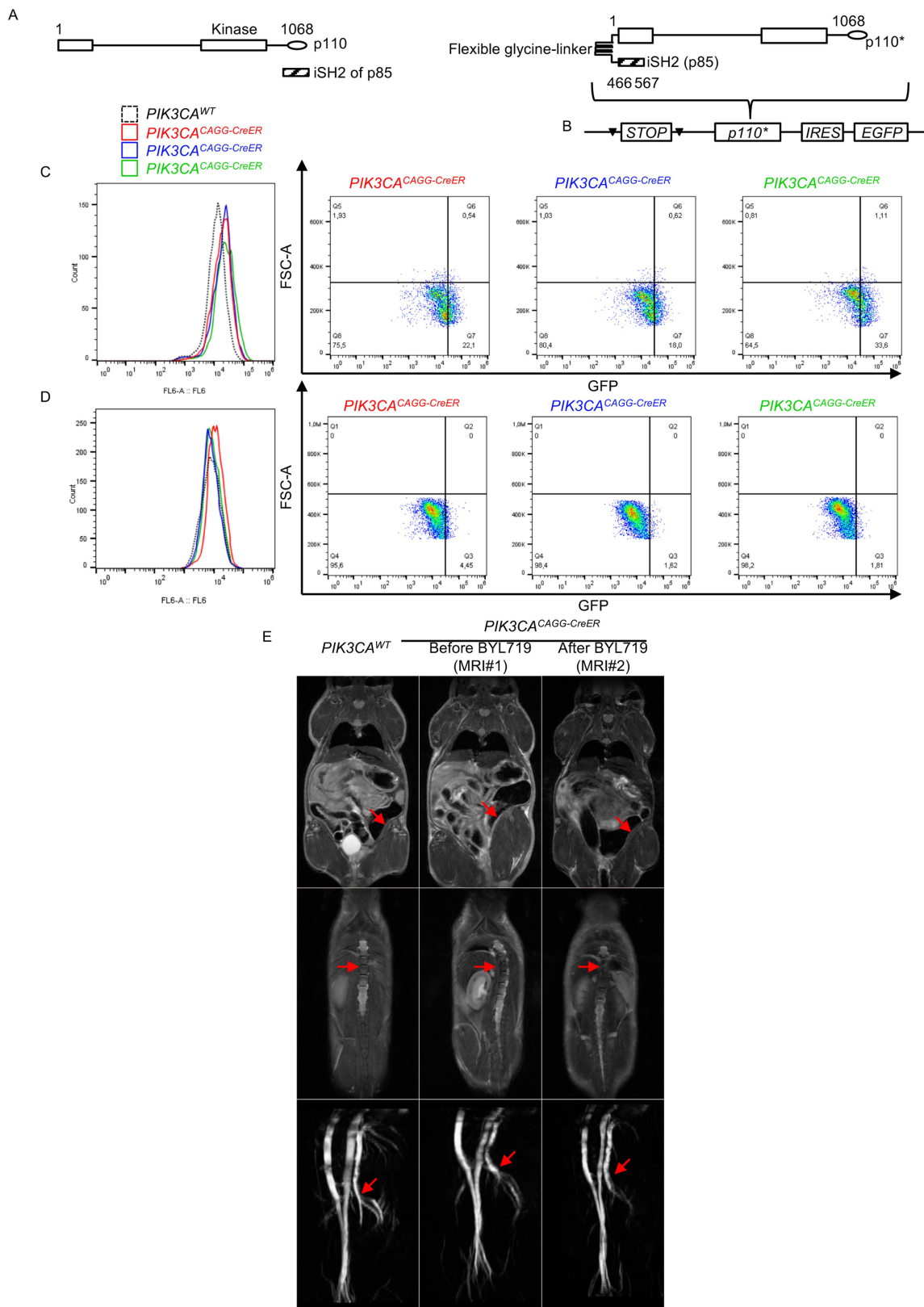
Patients were followed at regular intervals: weekly for eight weeks, every two weeks for one month and then monthly. Glycaemia was evaluated daily for the first month and then progressively less frequently. At all time points, the patients had a physical examination and performance status measurement using the Karnofsky (on a scale from 0 to 100, with lower numbers indicating greater disability) and ECOG indexes (a scale of 0 to 5, with 0 indicating no symptoms and higher scores indicating increasing symptoms)^{23,24}. Growth of the children was monitored at all clinical appointments. Blood sampling (complete blood count, kidney and liver functions, glycated haemoglobin measurement) were performed at each time points. Glycaemia was monitored after all meals for two months and then the monitoring became progressively less frequent. Adverse events were graded according to National Cancer Institute Common Terminology Criteria for Adverse Events, version 4.0. All patients had heart ultrasound examination before BYL719 treatment and then every three months. Magnetic resonance imaging studies were performed before BYL719 introduction and then after three and six months of treatment. PET scans were performed before and at 3 months of treatment.

Data analysis and statistics. Data are expressed as mean ± s.e.m. Survival curves were analysed with the Mantel–Cox (log-rank) test. Differences between the experimental groups were evaluated using ANOVA, followed when significant ($P < 0.05$) with the Tukey–Kramer test. When only two groups were compared, Mann–Whitney tests were used. Statistical analyses were performed using GraphPad Prism software.

Reporting summary. Further information on experimental design is available in the Nature Research Reporting Summary linked to this paper.

Data availability. All data generated or analysed during this study are included in this published article (and its Supplementary Information Files).

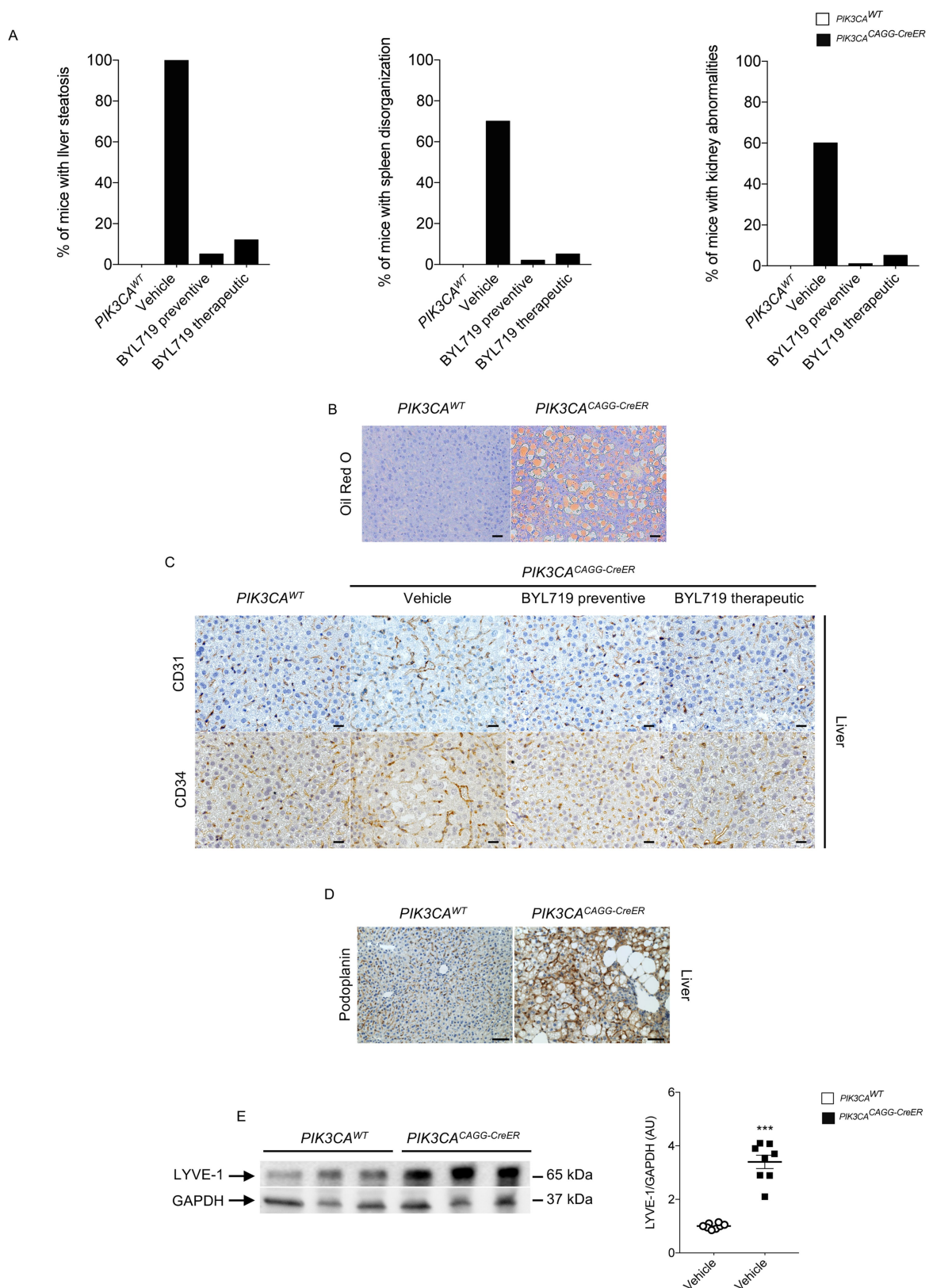
25. Seluanov, A., Vaidya, A. & Gorbunova, V. Establishing primary adult fibroblast cultures from rodents. *J. Vis. Exp.* **2010**, 2033 (2010).
26. Vandesompele, J. et al. Accurate normalization of real-time quantitative RT-PCR data by geometric averaging of multiple internal control genes. *Genome Biol.* **3**, RESEARCH0034 (2002).
27. Canaud, G. et al. Inhibition of the mTORC pathway in the antiphospholipid syndrome. *N. Engl. J. Med.* **371**, 303–312 (2014).



Extended Data Fig. 1 | See next page for caption.

Extended Data Fig. 1 | p110* construction and mouse model characterization. **a**, Left, Representation of p110 and iSH2 domain of the p85 subunit (striped bar). The iSH2 domain is important to stabilize the p110 α protein. The p110* protein is a constitutively active chimera that contains the iSH2 domain of p85 fused to the N terminus of p110 via a flexible glycine linker¹⁴ (right). **b**, To generate tissue-specific p110*-transgenic mice, a cloned loxP-flanked neoR-stop cassette was inserted into a modified version of pROSA26-1 followed by the cDNA encoding p110* and then a frt-flanked IRES-EGFP cassette and a bovine polyadenylation sequence (*R26StopFLP110**)¹³. **c**, **d**, EGFP expression from flow cytometry experiments in the spleen of *PIK3CA*^{WT}

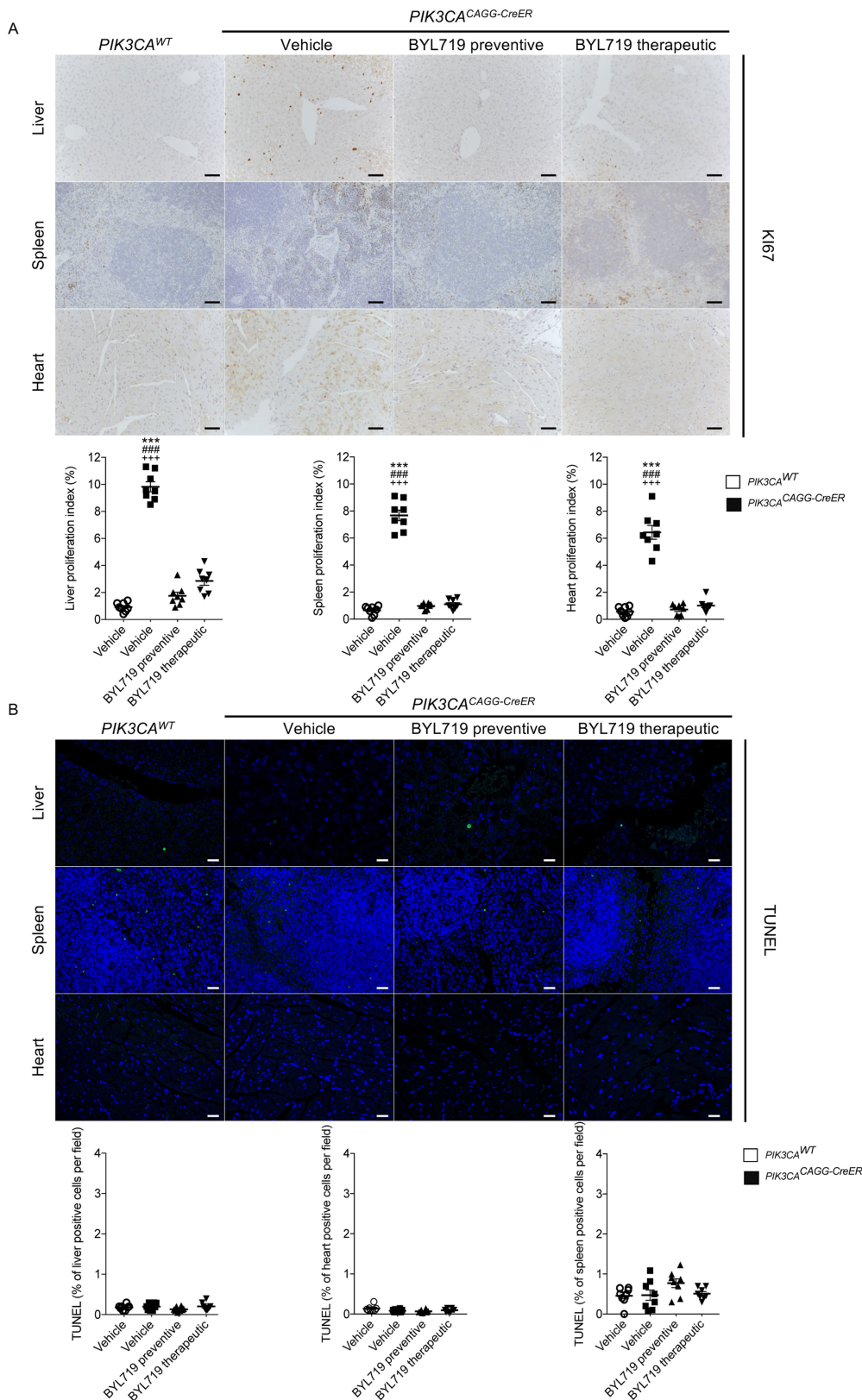
mice ($n = 12$) and *PIK3CA*^{CAGG-CreER} mice injected with either a single 40 mg kg⁻¹ dose (**c**; $n = 6$ mice) or a single 4 mg kg⁻¹ dose (**d**; $n = 6$ mice) of tamoxifen. Each curve is a different mouse. **e**, MRI examination of the PROS mouse model and efficacy of BYL719 treatment. Top, arrows show muscle hypertrophy in *PIK3CA*^{CAGG-CreER} mice before BYL719 treatment. This phenotype was reversed by BYL719 administration. Middle, arrows show scoliosis in *PIK3CA*^{CAGG-CreER} mice before BYL719 treatment, which was rescued by BYL719 administration. Bottom, arrows show arterial dilation in *PIK3CA*^{CAGG-CreER} mice before BYL719 treatment, which was reversed by BYL719 administration ($n = 6$ mice per group).



Extended Data Fig. 2 | Quantification and vessel malformation.

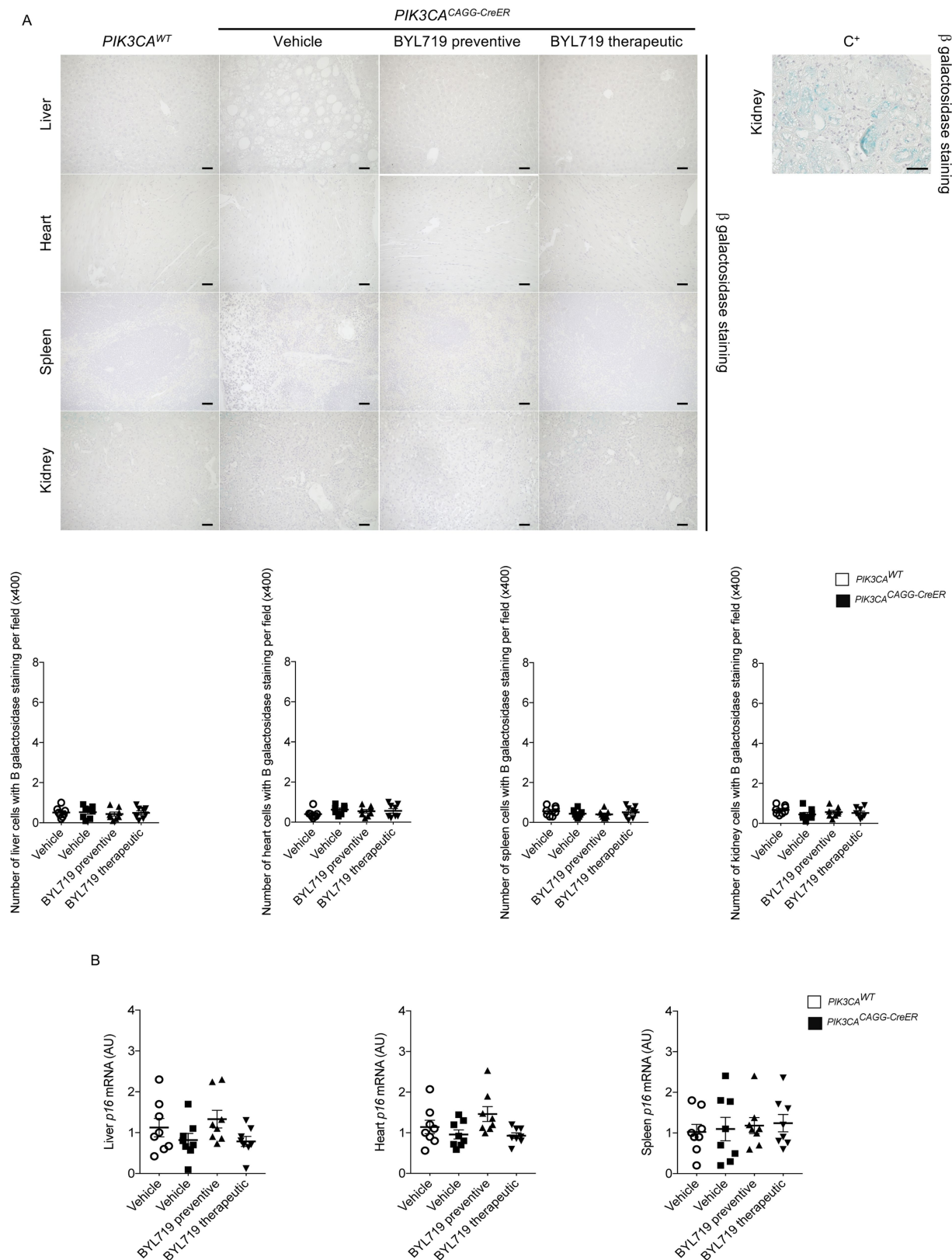
a, Percentage of $PIK3CA^{WT}$ and $PIK3CA^{CAGG-CreER}$ mice with or without BYL719 treatment presenting organ abnormalities. **b**, Oil Red O staining of the livers of $PIK3CA^{WT}$ and $PIK3CA^{CAGG-CreER}$ mice demonstrating steatosis ($n = 8$ mice per group). Scale bars, $10\ \mu\text{m}$. **c**, CD31 (top) and CD34 (bottom) immunostaining in the liver of $PIK3CA^{WT}$ and $PIK3CA^{CAGG-CreER}$ mice with or without BYL719 ($n = 8$ mice per group). $PIK3CA^{CAGG-CreER}$ mice treated with vehicle showed vessel dilation that was prevented or reversed by BYL719. Scale bars, $10\ \mu\text{m}$. **d**, Representative

picture of lymphatic malformation as assessed by podoplanin immunostaining in the liver of $PIK3CA^{WT}$ and $PIK3CA^{CAGG-CreER}$ mice ($n = 8$ mice per group). Scale bars, $10\ \mu\text{m}$. **e**, Representative western blot of LYVE-1 in the liver of $PIK3CA^{WT}$ and $PIK3CA^{CAGG-CreER}$ mice demonstrating lymphatic increased in the $PIK3CA^{CAGG-CreER}$ mice ($n = 8$ mice per group). All data are shown as the means \pm s.e.m. Mann-Whitney test (two-tailed, $P = 0.001$). $PIK3CA^{CAGG-CreER}$ versus $PIK3CA^{WT}$ mice, $***P < 0.001$.



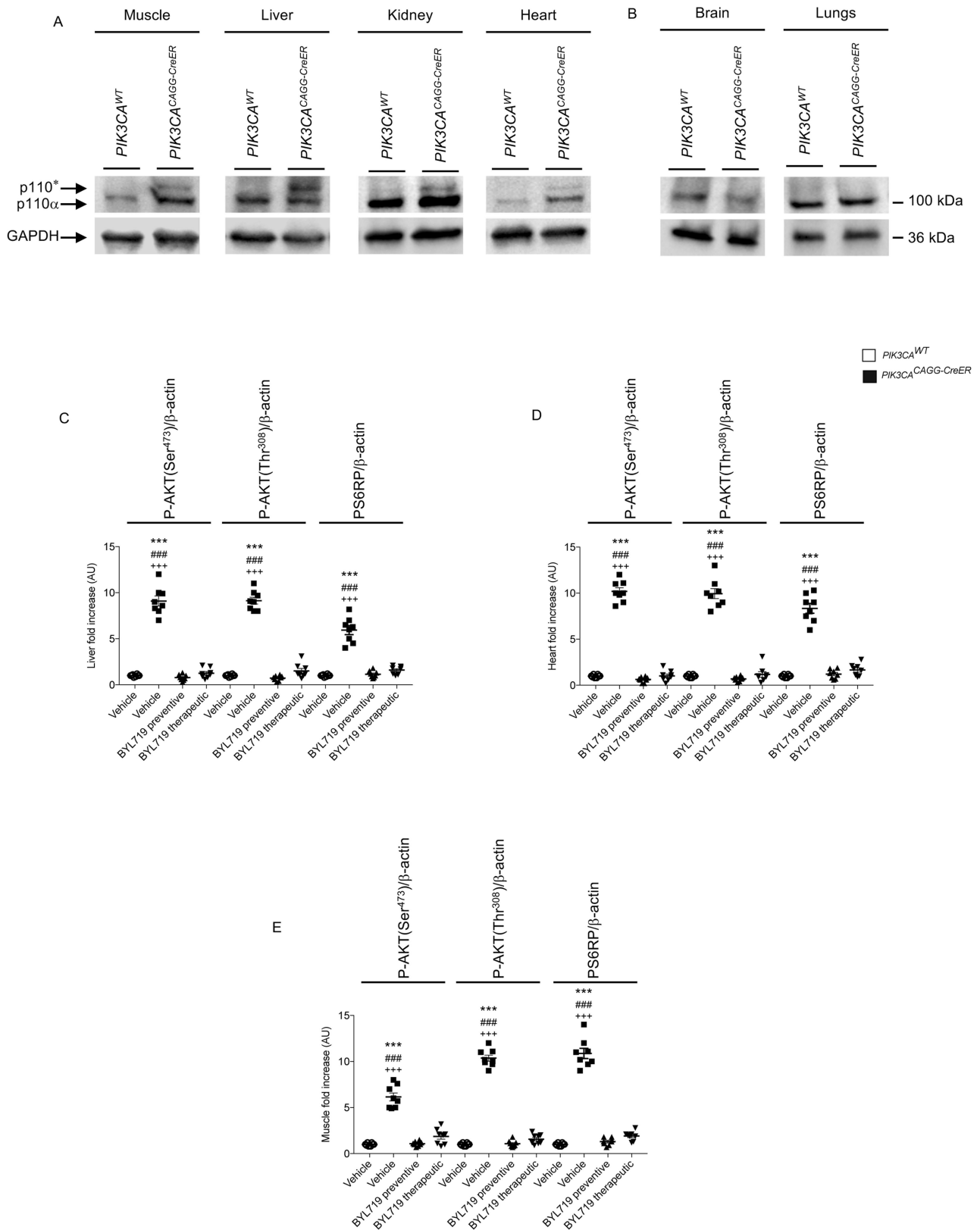
Extended Data Fig. 3 | BYL719 affects proliferation. **a**, Ki67 immunostaining and quantification in liver, spleen and heart of *PIK3CA*^{WT} and *PIK3CA*^{CAGG-CreER} mice with or without BYL719 treatment ($n = 8$ mice per group, 10 randomly selected fields per mouse, $\times 400$). **b**, TUNEL assay. The graphs show the quantification of TUNEL-positive cells per field ($n = 8$ mice per group, 10 randomly selected fields per mouse, $\times 400$).

Scale bars, 10 μ m. All data are shown as mean \pm s.e.m. ANOVA followed by Tukey–Kramer test (two-tailed). *PIK3CA*^{CAGG-CreER} versus *PIK3CA*^{WT} mice, $***P < 0.001$. *PIK3CA*^{CAGG-CreER} mice treated with vehicle versus *PIK3CA*^{CAGG-CreER} mice treated with preventive BYL719, $***P < 0.001$. *PIK3CA*^{CAGG-CreER} mice treated with vehicle versus *PIK3CA*^{CAGG-CreER} mice treated with therapeutic BYL719, $+++P < 0.001$.



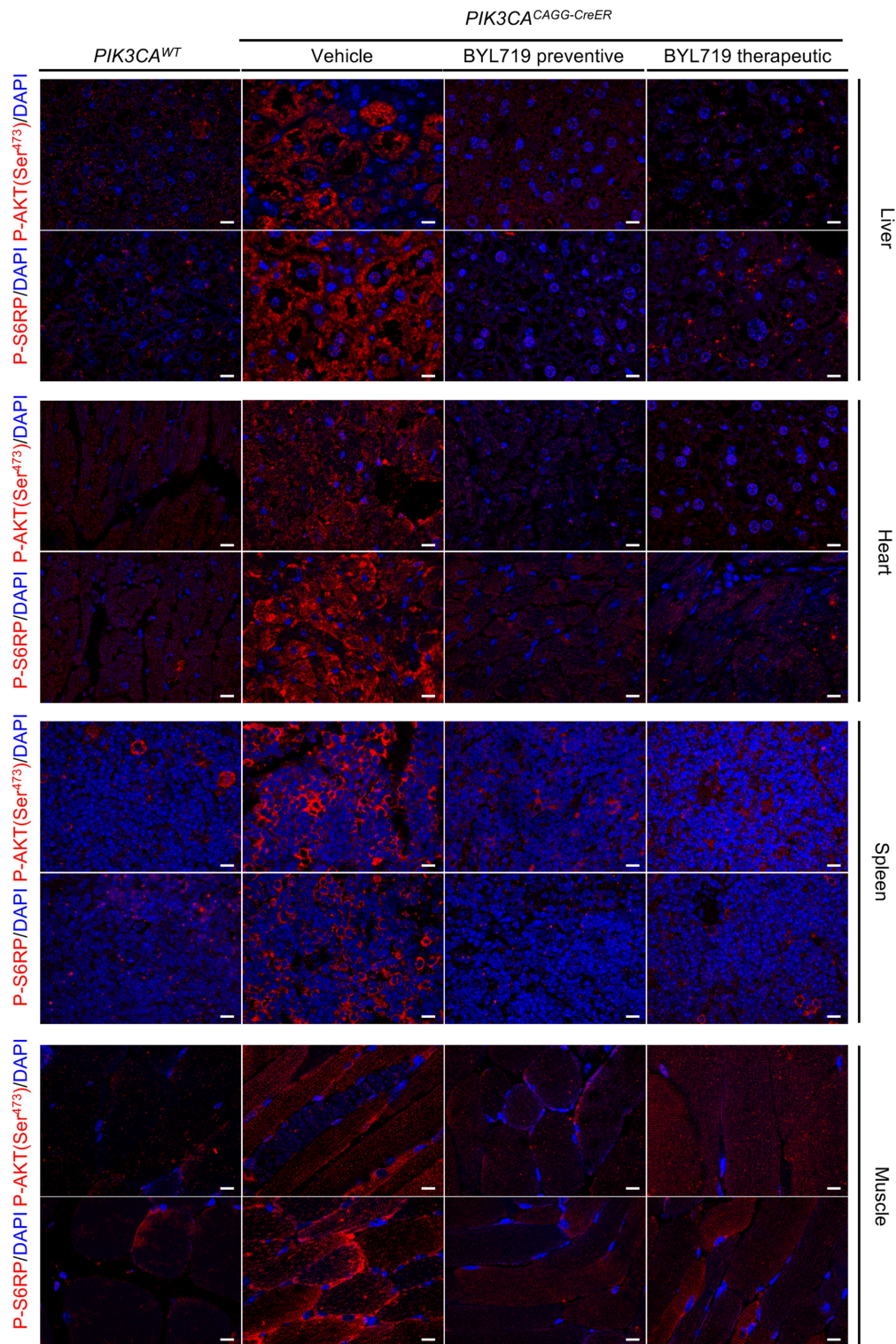
Extended Data Fig. 4 | Senescence and BYL719. **a**, β -galactosidase staining in the liver, heart, spleen and kidney of *PIK3CA*^{WT} and *PIK3CA*^{CAGG-CreER} mice with or without BYL719 and quantification of β -galactosidase-positive cells per field ($n = 8$ mice per group, 10 randomly selected fields, $\times 400$). C⁺: positive control. Scale bars, 10 μ m.

b, *p16* mRNA expression in liver, heart and spleen of *PIK3CA*^{WT} and *PIK3CA*^{CAGG-CreER} mice treated with or without BYL719 ($n = 8$ mice per group). A.U., arbitrary unit. All data are shown as mean \pm s.e.m. ANOVA followed by Tukey–Kramer test (two-tailed).



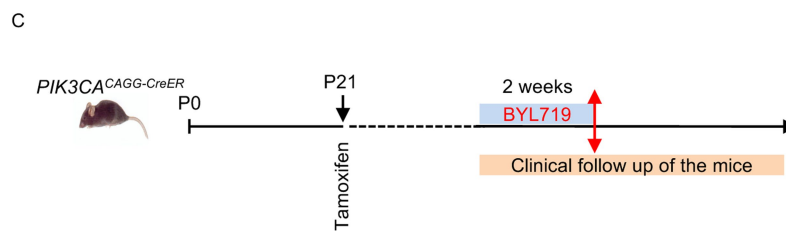
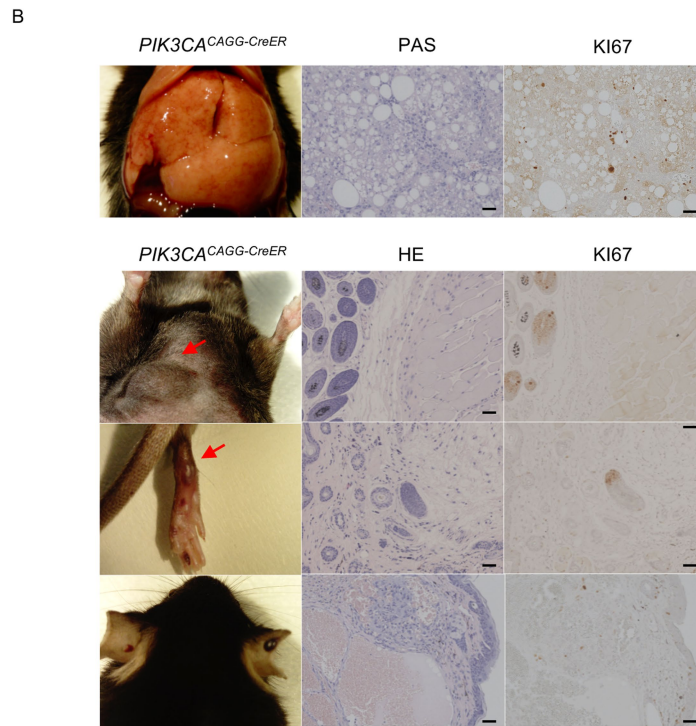
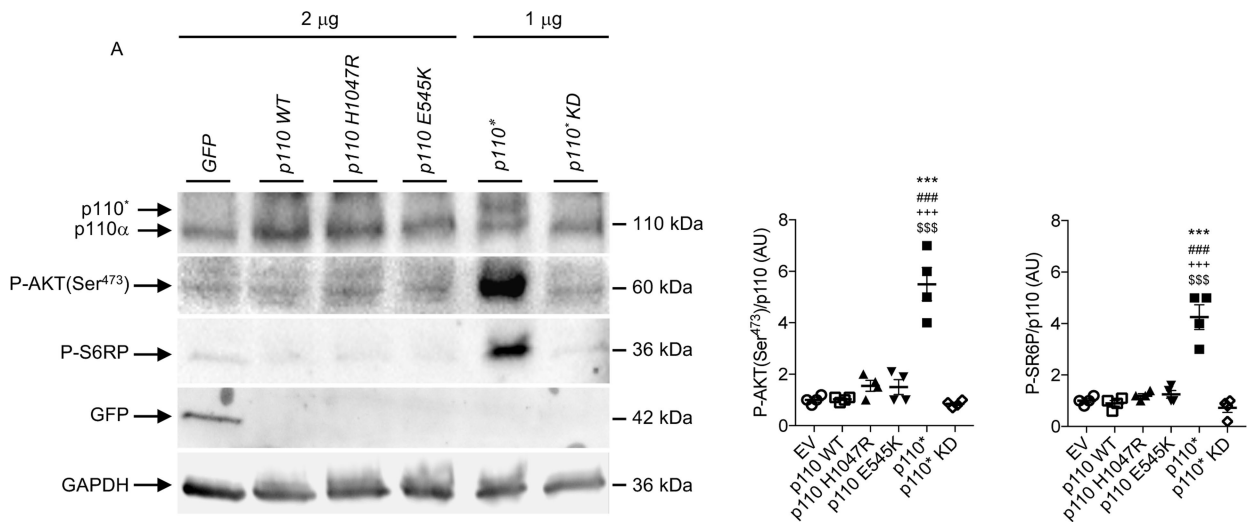
Extended Data Fig. 5 | p110* expression in affected tissues. **a**, Western blot showing the expression of p110* in *PIK3CA*^{CAGG-CreER} mice ($n = 8$ mice per group). **b**, p110* is not expressed in the brain or lungs ($n = 8$ mice per group). **c–e**, Western blot quantification of Fig. 1d, in the liver (**c**), heart (**d**) and muscle (**e**) of *PIK3CA*^{WT} and *PIK3CA*^{CAGG-CreER} mice treated with or without BYL719 ($n = 8$ mice per group). All data are shown as

mean \pm s.e.m. ANOVA followed by Tukey–Kramer test (two-tailed). *PIK3CA*^{CAGG-CreER} versus *PIK3CA*^{WT} mice, *** $P < 0.001$. *PIK3CA*^{CAGG-CreER} mice treated with vehicle versus *PIK3CA*^{CAGG-CreER} mice treated with preventive BYL719, ### $P < 0.001$. *PIK3CA*^{CAGG-CreER} mice treated with vehicle versus *PIK3CA*^{CAGG-CreER} mice treated with therapeutic BYL719, +++ $P < 0.001$.



Extended Data Fig. 6 | Ability of BYL719 to inhibit PIK3CA activation in different tissues. Immunofluorescence staining of P-AKT (Ser⁴⁷³) and P-S6RP in the liver (a), heart (b), spleen (c) and muscles (d) of *PIK3CA^{WT}*

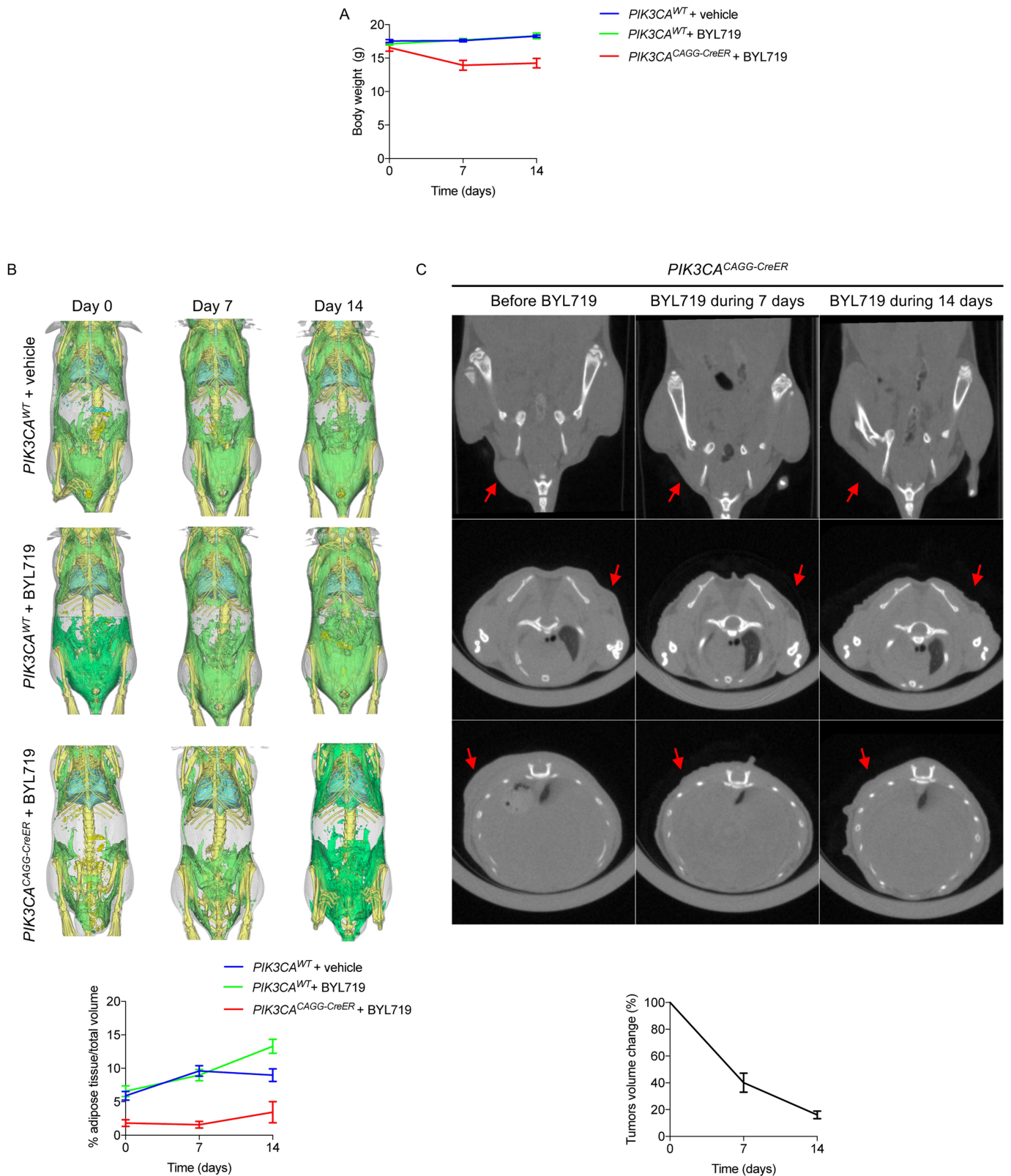
and *PIK3CA^{CAGG-CreER}* mice treated with or without BYL719 ($n = 8$ mice per group). Scale bars, 10 μm .



Extended Data Fig. 7 | See next page for caption.

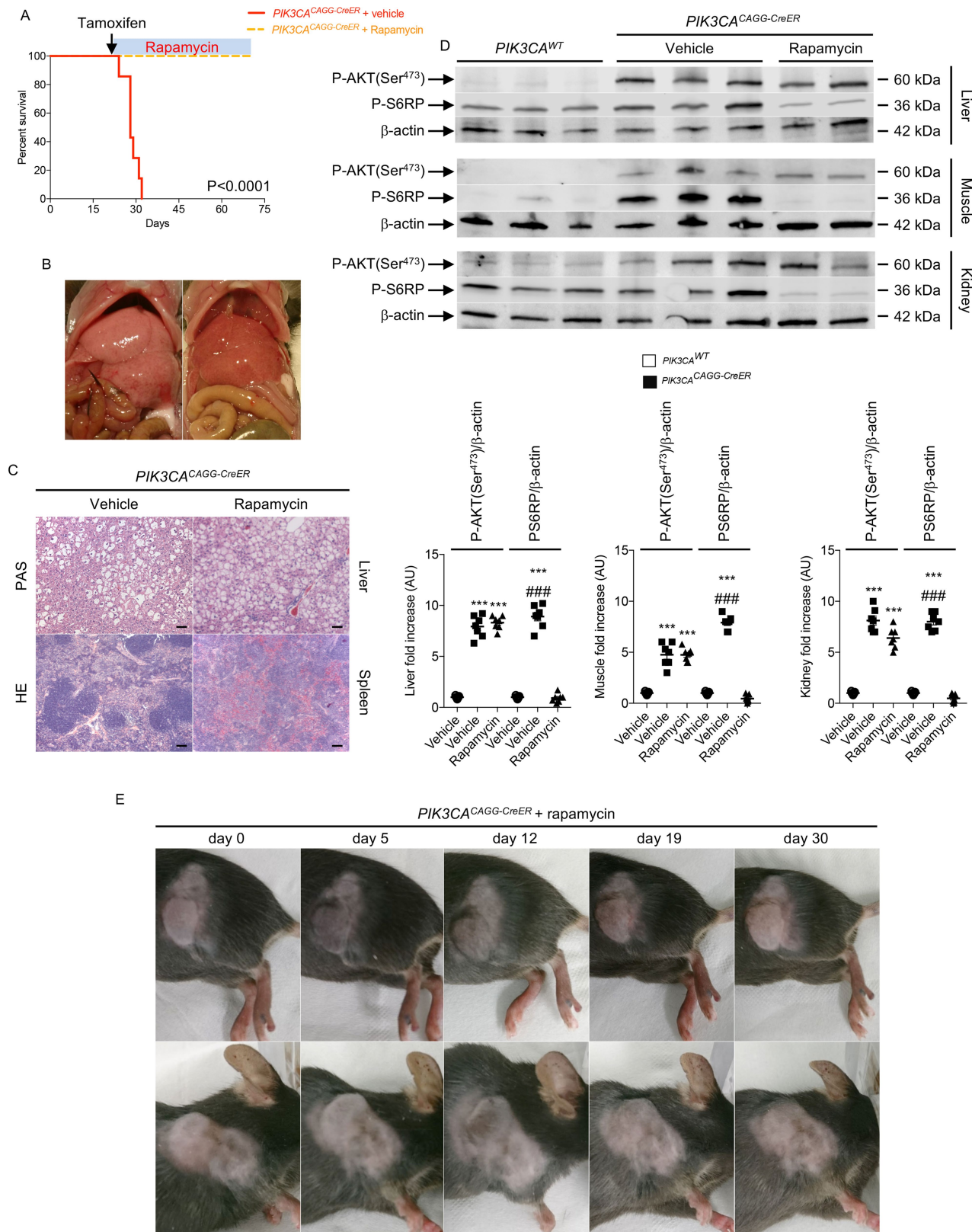
Extended Data Fig. 7 | Recruitment of the AKT/mTORC pathway by the different forms of mutant p110. **a**, Western blot and quantification of p110, P-AKT (Ser⁴⁷³), P-S6RP and GFP in HeLa cells transfected with plasmids containing cDNA encoding p110*, p110* kinase-dead mutant (p110* KD) as a control, H1047R mutation or E545K mutation. Cells transfected with the p110* mutant showed a more powerful effect on the activation of the AKT/mTORC pathway than the others ($n = 4$ independent experiments). All data are shown as mean \pm s.e.m. ANOVA followed by Tukey–Kramer test (two-tailed). p110* versus H1047R mutation, *** $P < 0.001$. p110* versus E545K mutation, ### $P < 0.001$.

p110* versus wild-type p110, +++ $P < 0.001$. p110* versus p110* KD, §§§ $P < 0.001$. Negative control is a vector that contains cDNA encoding GFP. **b**, Histological examination of different tissues from *PIK3CA*^{CAGG-CreER} mice. Left column, from top to bottom, liver, abdominal tumour, leg and ear abnormalities. Middle column, PAS or HE staining of the tissue. Right column, Ki67 staining of the same tissue ($n = 8$ mice). Scale bars, 20 μ m. **c**, Design of the experiment shown in Fig. 2h. *PIK3CA*^{CAGG-CreER} mice received a single dose of 4 mg kg⁻¹ tamoxifen and were followed for one month. Once the tumours became visible, BYL719 was started for two weeks and then withdrawn.



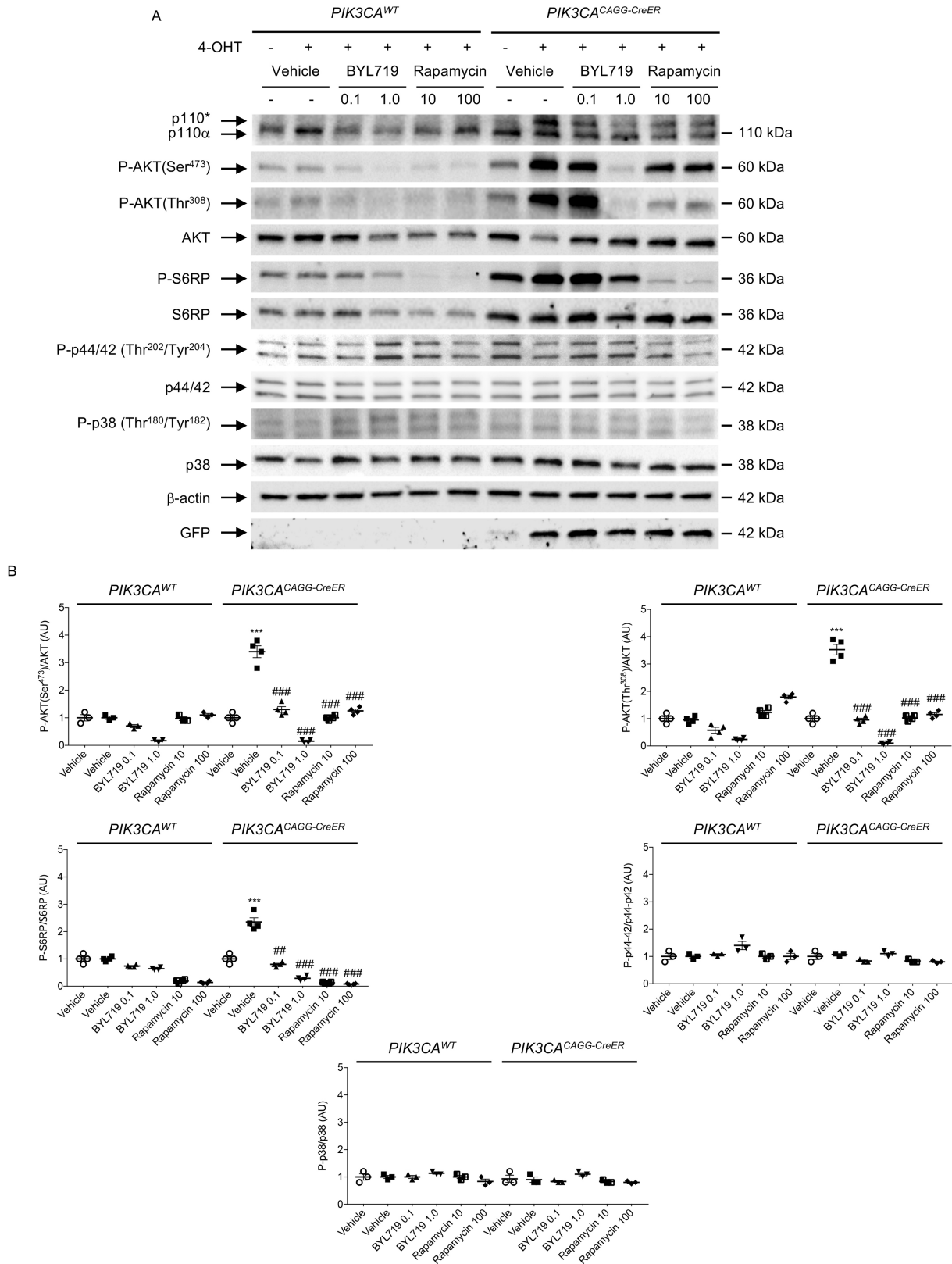
Extended Data Fig. 8 | CT scan evaluation of the tumours and adipose tissue before and after BYL719 introduction. a, Body weight evolution of *PIK3CA*^{WT} and *PIK3CA*^{CAGG-CreER} mice treated with vehicle or BYL719 (*n* = 3 mice per group). **b,** CT scan evaluation and quantification of the fat tissue content in *PIK3CA*^{WT} and *PIK3CA*^{CAGG-CreER} mice treated with vehicle or BYL719. Subcutaneous and visceral fat content were measured

before treatment and 7 and 14 days after onset of treatment with vehicle or BYL719 (*n* = 3 mice per group). **c,** CT scan evaluation and quantification of tumour volume in *PIK3CA*^{CAGG-CreER} mice before and after two weeks of BYL719 treatment (arrows) (*n* = 3 mice per group). All data are shown as mean ± s.e.m.



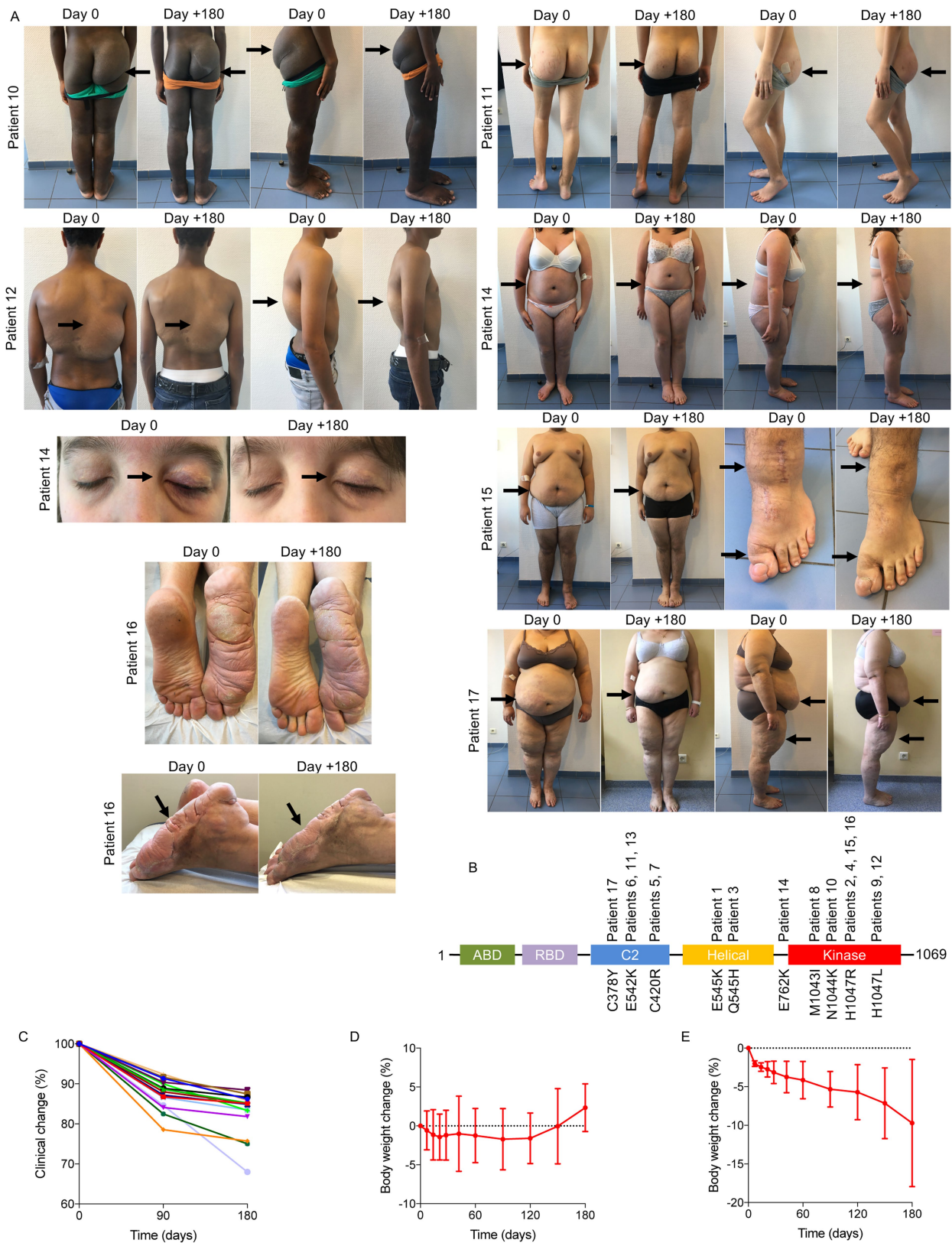
Extended Data Fig. 9 | Effect of rapamycin treatment on the different *PIK3CA*^{CAGG-CreER} mouse models. a, Kaplan–Meier survival curves of *PIK3CA*^{CAGG-CreER} mice that received a single dose of 40 mg kg⁻¹ tamoxifen and were treated with or without rapamycin after tamoxifen administration. **b**, Representative pictures of the liver of *PIK3CA*^{CAGG-CreER} mice treated with rapamycin 40 days after *Cre* induction. **c**, Morphology of livers and spleens from *PIK3CA*^{WT} and *PIK3CA*^{CAGG-CreER} mice that were treated with or without rapamycin after *Cre* induction. Scale bars, 10 μm. **d**, Western blot and quantification of P-AKT (Ser⁴⁷³) and P-S6RP in the

liver, heart and muscle, respectively, of *PIK3CA*^{WT} and *PIK3CA*^{CAGG-CreER} mice treated with vehicle or rapamycin directly after *Cre* induction. **e**, *PIK3CA*^{CAGG-CreER} mice were treated with rapamycin one month after *Cre* induction with a single dose of 4 mg kg⁻¹ tamoxifen and followed for one month. All data are shown as mean ± s.e.m. ANOVA followed by Tukey–Kramer test (two-tailed). *PIK3CA*^{CAGG-CreER} versus *PIK3CA*^{WT} mice, ****P* < 0.001. *PIK3CA*^{CAGG-CreER} mice treated with rapamycin compared with *PIK3CA*^{CAGG-CreER} mice treated with vehicle, ###*P* < 0.001.



Extended Data Fig. 10 | In vitro effect of BYL719 and rapamycin on fibroblasts from *PIK3CA^{CAGG-CreER}* mice. a, Skin fibroblasts from *PIK3CA^{WT}* and *PIK3CA^{CAGG-CreER}* mice were isolated and exposed to vehicle or increasing concentrations of BYL719 or rapamycin for 24 h. b, Quantification. White column, without 4-OHT; black column, with

4-OHT. All data are shown as mean ± s.e.m. ANOVA followed by Tukey-Kramer test (two-tailed). Before versus after *Cre* induction with 4-OHT, ****P* < 0.001. BYL719 or rapamycin exposure compared with cells treated with vehicle, ***P* < 0.01 and #*P* < 0.001.

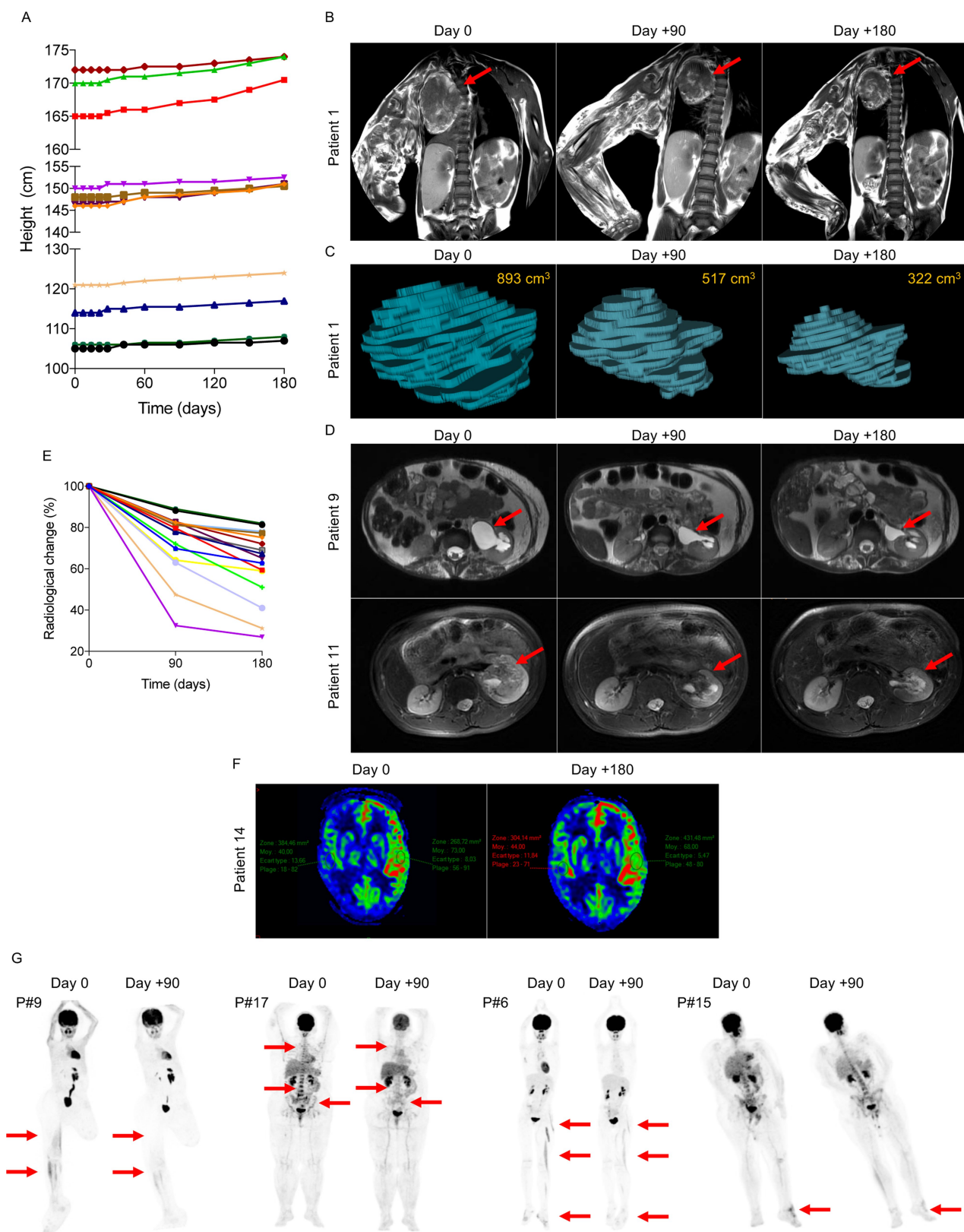


Extended Data Fig. 11 | See next page for caption.

Extended Data Fig. 11 | Effect of BYL719 in patients with PROS.

a, Patients 10–17 before and after 180 days of BYL719 treatment. Patient 10 was a 14-year-old boy with severe asthenia, dyspnea and bilateral overgrowth of lower limbs. After 180 days of treatment asthenia resolved and we observed a marked reduction in hypertrophy of the limbs. Patient 11 was a 14-year-old boy with overgrowth of the right buttock and an intra-abdominal vascular tumour infiltrating the left kidney and spinal nerve. He had chronic haematuria and was permanently confined to bed owing to pain. After 180 days, haematuria resolved and the volume of the intraabdominal vascular malformation was reduced by up to 68%. He had no more pain and became capable of walking. Patient 12 was a 15-year-old boy with multiple large tumours of the trunk and the back. After 180 days of treatment the tumours had reduced in size. Patient 13 was a 16-year-old boy with megalencephaly-capillary malformation (MCAP) and left hemifacial hyperplasia. Treatment led to a reduction in hemifacial hypertrophy and cognitive improvement. Owing to the deformation, this patient was not able to open the left eye. After 180 days of BYL719 treatment, he was able to open the eye (not shown for confidentiality reasons). Patient 14 was a 16-year-old girl with MCAP and a chronic noninfectious palpebral cellulitis who was steroid-dependent. BYL719 treatment led to the healing of the cellulitis and steroids were

stopped without a flare. We also observed enhancement of cognitive function and behaviour and improvement of scoliosis. Patient 15 was a 19-year-old man with overgrowth of the left foot and unstable and painful walking. Treatment led to an improvement in the overgrowth as well as an improvement in walking distance. Patient 16 was a 32-year-old man with overgrowth of the right foot and unstable and painful walking. Treatment led to an improvement in the overgrowth as well as an improvement in walking distance. Patient 17 was 50-year-old woman with generalized hypertrophy, and severe and diffuse pain with opioid dependency. She was permanently confined to bed. After six months of treatment we observed an improvement in tiredness, and resolution of pain, and we were able to stop opioids within two weeks. The patient became able to walk again. **b**, *PIK3CA* mutations identified in the 17 patients. **c**, For each patient we determined a target lesion (see Supplementary Table 2) that was clinically measured at each time point. The graph represents the changes (per cent) during the 180 days of treatment with BYL719. Each line is a single patient. **d**, Mean body weight changes (per cent) during the 180 days of treatment with BYL719 ($n = 13$ patients, patients 1–13), excluding the four obese patients (patients 14, 15, 16 and 17). **e**, Mean body weight loss in the four obese patients during the 180 days of treatment with BYL719. All data are shown as mean \pm s.e.m.



Extended Data Fig. 12 | Height changes in children during treatment period and radiological changes with BYL719 treatment. **a**, Height changes in children during the 180 days of treatment with BYL719. **b**, MRI scans of patient 1 before and after 180 days of BYL719 treatment. Arrows show the target lesion. **c**, Three-dimensional MRI-based reconstruction of the chest tumour in patient 1 before and after 180 days of BYL719 treatment. **d**, Examples of MRI showing the evolution of the target lesions

in patients 9 and 11. **e**, Volume evolution of the radiological target lesion after 180 days of BYL719 treatment. **f**, Diffusion MRI demonstrating the enhancement of brain perfusion in patient 14 after 180 days of BYL719. **g**, PET scan images of patients 6, 9, 15 and 17, before and after 90 days of BYL719 treatment. The arrows delineate hypermetabolic activity before and after 90 days of treatment.

Reporting Summary

Nature Research wishes to improve the reproducibility of the work that we publish. This form provides structure for consistency and transparency in reporting. For further information on Nature Research policies, see [Authors & Referees](#) and the [Editorial Policy Checklist](#).

Statistical parameters

When statistical analyses are reported, confirm that the following items are present in the relevant location (e.g. figure legend, table legend, main text, or Methods section).

n/a Confirmed

- The exact sample size (n) for each experimental group/condition, given as a discrete number and unit of measurement
- An indication of whether measurements were taken from distinct samples or whether the same sample was measured repeatedly
- The statistical test(s) used AND whether they are one- or two-sided
Only common tests should be described solely by name; describe more complex techniques in the Methods section.
- A description of all covariates tested
- A description of any assumptions or corrections, such as tests of normality and adjustment for multiple comparisons
- A full description of the statistics including central tendency (e.g. means) or other basic estimates (e.g. regression coefficient) AND variation (e.g. standard deviation) or associated estimates of uncertainty (e.g. confidence intervals)
- For null hypothesis testing, the test statistic (e.g. F , t , r) with confidence intervals, effect sizes, degrees of freedom and P value noted
Give P values as exact values whenever suitable.
- For Bayesian analysis, information on the choice of priors and Markov chain Monte Carlo settings
- For hierarchical and complex designs, identification of the appropriate level for tests and full reporting of outcomes
- Estimates of effect sizes (e.g. Cohen's d , Pearson's r), indicating how they were calculated
- Clearly defined error bars
State explicitly what error bars represent (e.g. SD, SE, CI)

Our web collection on [statistics for biologists](#) may be useful.

Software and code

Policy information about [availability of computer code](#)

Data collection

Provide a description of all commercial and custom code used to collect the data in this study, specifying the version used OR state that no software was used.

Data analysis

Graph Prism software

For manuscripts utilizing custom algorithms or software that are central to the research but not yet described in published literature, software must be made available to editors/reviewers upon request. We strongly encourage code deposition in a community repository (e.g. GitHub). See the Nature Research [guidelines for submitting code & software](#) for further information.

Data

Policy information about [availability of data](#)

All manuscripts must include a [data availability statement](#). This statement should provide the following information, where applicable:

- Accession codes, unique identifiers, or web links for publicly available datasets
- A list of figures that have associated raw data
- A description of any restrictions on data availability

Provide your data availability statement here.

Field-specific reporting

Please select the best fit for your research. If you are not sure, read the appropriate sections before making your selection.

Life sciences Behavioural & social sciences

For a reference copy of the document with all sections, see [nature.com/authors/policies/ReportingSummary-flat.pdf](https://www.nature.com/authors/policies/ReportingSummary-flat.pdf)

Life sciences

Study design

All studies must disclose on these points even when the disclosure is negative.

Sample size	Sizes were defined to have sufficient statistical power
Data exclusions	No data exclusion
Replication	All experiments were performed at least four times and in duplicate
Randomization	Mice were randomly assigned to placebo or treatment
Blinding	All experiments were analyzed blindly

Materials & experimental systems

Policy information about [availability of materials](#)

n/a	Involved in the study
<input type="checkbox"/>	<input type="checkbox"/> Unique materials
<input type="checkbox"/>	<input checked="" type="checkbox"/> Antibodies
<input checked="" type="checkbox"/>	<input type="checkbox"/> Eukaryotic cell lines
<input type="checkbox"/>	<input checked="" type="checkbox"/> Research animals
<input type="checkbox"/>	<input checked="" type="checkbox"/> Human research participants

Unique materials

Obtaining unique materials *Describe any restrictions on the availability of unique materials OR confirm that all unique materials used are readily available from the authors or from standard commercial sources (and specify these sources).*

Antibodies

Antibodies used

Paraffin-embedded kidney sections (4- m) were incubated with anti-P-AKT (Ser473) antibody (Cell Signaling Technology, ref# 4060, dilution 1:100), anti-P-S6RP antibody (Cell Signaling Technology, ref# 5364, dilution 1:100), anti- -smooth muscle cell antibody (Sigma Aldrich, ref# A5228, dilution 1:100), anti-CD34 antibody (eBioscience, ref# 14-0341, dilution 1:100), anti-CD31 antibody (Dianova, ref# Dia-310, dilution 1:30) and anti-podoplanin antibody (Agilent, ref#M3619, dilution 1:50). Western blots were performed as previously described³⁰. Briefly, protein extracts from the liver, muscles, heart, kidneys and fibroblasts were resolved by SDS-PAGE before being transferred onto the appropriate membrane and incubated with anti-P-AKT (Ser473) antibody (Cell Signaling Technology, ref# 4060, dilution 1:1000), anti-P-AKT (Thr308) antibody (Cell Signaling Technology, ref# 13038, dilution 1:1000), anti- AKT antibody (Cell Signaling Technology, ref# 9272, dilution 1:1000), anti-P-S6RP antibody (Cell Signaling Technology, ref# 5364, dilution 1:1000), anti-p110 (Cell Signaling Technology, ref# 4249, dilution 1:1000), anti-LYVE-1 (R&D Systems, ref# AF2125, dilution 1:1000), anti-P-p44/42 antibody (Cell Signaling Technology, ref# 4370, dilution 1:1000), anti-p44/42 (Thr202/Tyr204) antibody (Cell Signaling Technology, ref# 9102, dilution 1:1000), anti-P-p38 (Thr180/Tyr182) antibody (Cell Signaling Technology, ref# 9216, dilution 1:1000), anti-p38 antibody (Cell Signaling Technology, ref# 8690, dilution 1:1000), anti-GFP antibody (Abcam, ref# ab13970, dilution 1:1000), anti-GAPDH (Merck Millipore, ref#374, dilution 1:1000) or anti- actin antibody (Sigma-Aldrich, ref#A2228, dilution 1:1000), followed by the appropriate peroxidase-conjugated secondary antibody (dilution 1:10000).

Validation

Describe the validation of each primary antibody for the species and application, noting any validation statements on the manufacturer's website, relevant citations, antibody profiles in online databases, or data provided in the manuscript.

Research animals

Policy information about [studies involving animals](#); [ARRIVE guidelines](#) recommended for reporting animal research

Animals/animal-derived materials

For this study, we interbred homozygous R26StopFLP110* (Stock# 012343) and heterozygous CAGGCre-ERTM (Stock# 004682) mice on the C57BL/6 background obtained from Jackson Laboratories. We obtained R26StopFLP110*+/- x CAGGCre-ERTM+ mice (referred here as PIK3CACAGG-CreER mice) and R26StopFLP110*+/- x CAGGCre-ERTM- mice (referred here as PIK3CAWT mice). We used the p110* construction published by Klippel A. et al17 (Supplementary Fig.1). The p110* protein is a constitutively active chimera that contains the iSH2 domain of p85 fused to the NH2-terminus of p110 via a flexible glycine-linker. To generate tissue-specific p110*-transgenic mice, a cloned loxP-flanked neoR-stop cassette was inserted into a modified version of pROSA26-1 followed by the cDNA encoding p110* and then a frt-flanked IRES-EGFP cassette and a bovine polyadenylation sequence (R26StopFLP110*)¹⁶.

Animals were fed ad libitum and housed at a constant ambient temperature in a 12-hour light cycle. Animal procedures were approved by the "Services Vétérinaires de la Préfecture de Police de Paris" Departmental Director and by the ethical committee of the Paris Descartes University. In the first study, a single dose of tamoxifen (40 mg.kg-1) was administered through oral gavage when the mice were at 21 days of age. For the survival studies, the mice were followed daily after tamoxifen gavage (PIK3CAWT n=16 and PIK3CACAGG-CreER n=16). For the preventive studies, the mice were treated with the PI3KCA inhibitor, BYL719 (MedChem Express; 50 mg.kg-1 in 0.5% carboxymethylcellulose (Sigma Aldrich), daily p.o.) (n=16) or vehicle (0.5% carboxymethylcellulose (Sigma Aldrich), daily p.o.) (n=16). For the therapeutic studies, the mice were treated with the PI3KCA inhibitor, BYL719 (MedChem Express; 50 mg.kg-1 in 0.5% carboxymethylcellulose (Sigma Aldrich), daily p.o.) (n=12) or vehicle (0.5% carboxymethylcellulose (Sigma Aldrich), daily p.o.) (n=12). Treatment was started at the same time of tamoxifen gavage, for the preventive study, or seven days after, for the therapeutic study.

In the second study, a single dose of tamoxifen (4 mg.kg-1) was administered through oral gavage when the mice were at 21 days of age (PIK3CACAGG-CreER n=28). Ten mice were sacrificed at approximately 1 month post tamoxifen gavage when tumors reached a certain volume for tissues examination. Once gross morphological abnormalities were visible, eighteen mice were treated with BYL719 during 15 days and treatment was stopped once macroscopic lesions disappeared to follow their phenotype.

In the third study, a single dose of tamoxifen (40 mg.kg-1) was administered through oral gavage when the mice were at 21 days of age and then were treated with daily intraperitoneal injection of rapamycin (MedChem Express, ref#HY-10219) (PIK3CACAGG-CreER n=7) or vehicle (PIK3CACAGG-CreER n=7) during 30 days. Rapamycin was dissolved to a final concentration of 0.5 mg.ml-1 in absolute ethanol dissolved further in 5% polyethylene glycol (PEG-400) and 5% Tween 80 in PBS and used for intraperitoneal injection at 4 mg.kg-1. All mice treated with rapamycin or vehicle were then sacrificed for tissues examination.

In the fourth study, a single dose of tamoxifen (4 mg.kg-1) was administered through oral gavage when the mice were at 21 days of age (PIK3CACAGG-CreER n=6). Once gross morphological abnormalities were visible (approximately 30 days later), all the mice were treated with daily intraperitoneal injection of rapamycin (MedChem Express, ref#HY-10219) during 30 days. Rapamycin was dissolved to a final concentration of 0.5 mg/ml in absolute ethanol dissolved further in 5% polyethylene glycol (PEG-400) and 5% Tween 80 in PBS and used for intraperitoneal injection at 4 mg.kg-1.

Human research participants

Policy information about [studies involving human research participants](#)

Population characteristics

The study was conducted on 19 patients, 4 adults and 15 children, followed at Necker hospital. This protocol was approved by the "Agence Nationale de Sécurité du Médicament et des Produits de Santé" (ANSM, authorizations n°: 553984-986, 584018, 585881-586135, 585464, 585465, 585467, 585880, 586136, 585463, 596229, 588018, 587904, 587896-912, 587908, 587905, 587910, 585458, 595374, 587899) and informed written consent was obtained from the adult patient and the legal representatives of the child. BYL719 was compassionately offered by Novartis. Adult patients received 250 mg/day and child patients received 50 mg/day. BYL719 was orally delivered every morning before breakfast.

Patients were followed at regular intervals: weekly during 8 weeks, every two weeks during 1 month and then monthly.

Glycaemia was evaluated daily the first month and then progressively sparse. At all time points, the patients had a physical examination and performance status measurement using the Karnofsky (on a scale from 0 to 100, with lower numbers indicating greater disability) and the ECOG indexes (a scale of 0 to 5, with 0 indicating no symptoms and higher scores indicating increasing symptoms)^{25,26}. Growth of the children was monitored at all clinical appointments. Blood sampling (complete blood count, kidney and liver functions, glycated hemoglobin measurement) were performed at each time points. Glycaemia was monitored after all meals over two months and then the monitoring became progressively sparse. Adverse events were graded according to National Cancer Institute Common Terminology Criteria for Adverse Events, version 4.0. All patients had heart ultrasound before BYL719 and then every 3 months. Magnetic resonance imaging studies were performed before BYL719 introduction and then at 3 and 6 months of treatment. PET-scan were performed before and at 3 months of treatment.

Method-specific reporting

n/a	Involvement in the study
<input checked="" type="checkbox"/>	<input type="checkbox"/> ChIP-seq
<input type="checkbox"/>	<input checked="" type="checkbox"/> Flow cytometry
<input type="checkbox"/>	<input checked="" type="checkbox"/> Magnetic resonance imaging

Flow Cytometry

Plots

Confirm that:

- The axis labels state the marker and fluorochrome used (e.g. CD4-FITC).
- The axis scales are clearly visible. Include numbers along axes only for bottom left plot of group (a 'group' is an analysis of identical markers).
- All plots are contour plots with outliers or pseudocolor plots.
- A numerical value for number of cells or percentage (with statistics) is provided.

Methodology

Sample preparation

Spleens of PIK3CAWT (n=12), PIK3CACAGG-CreER induced with tamoxifen 40 mg.kg⁻¹ (n=6) and PIK3CACAGG-CreER induced with tamoxifen 4 mg.kg⁻¹ (n=6) mice were mechanically disrupted in PBS/SVF 2%. Following dissociation, spleens were filtered, centrifuged and resuspended. Cells were then treated with a FC blocker for 10 min at 4°C (Biolegend, ref# 101302) and fixed/permeabilized (BD Bioscience, ref# 554714). Cells were labeled with chicken polyclonal anti-GFP antibody (Abcam, ref# ab13970) for 30 min at 4°C. Subsequently, cells were incubated with Alexa Fluor 647-labeled goat anti-chicken IgY antibody (Abcam, ref# ab150171) for 30 min at 4°C. A background control incubated only with secondary antibody was also included.

Instrument

Samples were analyzed using Gallios™ Flow Cytometer (Beckman Coulter)

Software

FlowJo software (TreeStar)

Cell population abundance

Describe the abundance of the relevant cell populations within post-sort fractions, providing details on the purity of the samples and how it was determined.

Gating strategy

Describe the gating strategy used for all relevant experiments, specifying the preliminary FSC/SSC gates of the starting cell population, indicating where boundaries between "positive" and "negative" staining cell populations are defined.

- Tick this box to confirm that a figure exemplifying the gating strategy is provided in the Supplementary Information.

Magnetic resonance imaging

Experimental design

Design type

MRI were performed at the Plateforme IRM, INSERM U970, Centre de recherche cardiovasculaire de Paris. Briefly, MRI were performed under general anesthesia in 4 weeks old female PIK3CAWT (n=6) and PIK3CACAGG-CreER (n=6) mice that received 7 days before a single dose of 40 mg.kg⁻¹ tamoxifen to induce Cre recombination. MRI were then repeated weekly in all mice during 1 month.

Design specifications

Specify the number of blocks, trials or experimental units per session and/or subject, and specify the length of each trial or block (if trials are blocked) and interval between trials.

Behavioral performance measures

State number and/or type of variables recorded (e.g. correct button press, response time) and what statistics were used to establish that the subjects were performing the task as expected (e.g. mean, range, and/or standard deviation across subjects).

Acquisition

Imaging type(s)

Whole body MRI

Field strength

Specify in Tesla

Sequence & imaging parameters

T1, T2

Area of acquisition

Whole body MRI

Diffusion MRI

Used

Not used

Preprocessing

Preprocessing software

Provide detail on software version and revision number and on specific parameters (model/functions, brain extraction, segmentation, smoothing kernel size, etc.).

Normalization

If data were normalized/standardized, describe the approach(es): specify linear or non-linear and define image types used for transformation OR indicate that data were not normalized and explain rationale for lack of normalization.

Normalization template

Describe the template used for normalization/transformation, specifying subject space or group standardized space (e.g. original Talairach, MNI305, ICBM152) OR indicate that the data were not normalized.

Noise and artifact removal

Describe your procedure(s) for artifact and structured noise removal, specifying motion parameters, tissue signals and physiological signals (heart rate, respiration).

Volume censoring

Define your software and/or method and criteria for volume censoring, and state the extent of such censoring.

Statistical modeling & inference

Model type and settings

Specify type (mass univariate, multivariate, RSA, predictive, etc.) and describe essential details of the model at the first and second levels (e.g. fixed, random or mixed effects; drift or auto-correlation).

Effect(s) tested

Define precise effect in terms of the task or stimulus conditions instead of psychological concepts and indicate whether ANOVA or factorial designs were used.

Specify type of analysis: Whole brain ROI-based BothAnatomical location(s) Statistic type for inference
(See [Eklund et al. 2016](#))

Specify voxel-wise or cluster-wise and report all relevant parameters for cluster-wise methods.

Correction

Describe the type of correction and how it is obtained for multiple comparisons (e.g. FWE, FDR, permutation or Monte Carlo).

Models & analysis

n/a | Involved in the study

 Functional and/or effective connectivity Graph analysis Multivariate modeling or predictive analysis

Functional and/or effective connectivity

Report the measures of dependence used and the model details (e.g. Pearson correlation, partial correlation, mutual information).